

# Surface Texturing of Prosthetic Hip Implant Bearing Surfaces: A Review

Quentin Allen

Department of Mechanical Engineering,  
University of Utah,  
1495 E. 100 S. (1550 MEK),  
Salt Lake City, UT 84112  
e-mail: q.s.allen@utah.edu

Bart Raeymaekers<sup>1</sup>

Department of Mechanical Engineering,  
University of Utah,  
1495 E. 100 S. (1550 MEK),  
Salt Lake City, UT 84112  
e-mail: bart.raeymaekers@utah.edu

*More than 300,000 total hip replacement surgeries are performed in the United States each year to treat degenerative joint diseases that cause pain and disability. The statistical survivorship of these implants declines significantly after 15–25 years of use because wear debris causes inflammation, osteolysis, and mechanical instability of the implant. This limited longevity has unacceptable consequences, such as revision surgery to replace a worn implant, or surgery postponement, which leaves the patient in pain. Innovations such as highly cross-linked polyethylene and new materials and coatings for the femoral head have reduced wear significantly, but longevity remains an imminent problem. Another method to reduce wear is to add a patterned microtexture composed of micro-sized texture features to the smooth bearing surfaces. We critically review the literature on textured orthopedic biomaterial surfaces in the context of prosthetic hip implants. We discuss the different functions of texture features by highlighting experimental and simulated results documented by research groups active in this area. We also discuss and compare different manufacturing techniques to create texture features on orthopedic biomaterial surfaces and emphasize the key difficulties that must be overcome to produce textured prosthetic hip implants. [DOI: 10.1115/1.4048409]*

*Keywords:* surface texture, lubrication, hip implant, artificial joints, bio-tribology

## 1 Introduction

Total hip replacement (THR) is one of the most common surgical procedures in the United States, during which a surgeon replaces a diseased or damaged hip joint with a prosthetic hip implant. The National Inpatient Sample (NIS) recorded 370,770 THR surgeries in 2014 (latest publicly available information) and projections estimate 635,000 THR surgeries per year in the US by 2030 [1], driven by an aging population, and the success of this surgery leading the trend for ever younger patients to undergo THR to relieve chronic joint pain [2]. Figure 1(a) schematically depicts a human hip joint, showing the femur, pelvis, and articular cartilage, whereas Fig. 1(b) schematically shows a prosthetic hip implant, modified from Ref. [3].

A prosthetic hip implant comprises a femoral head that attaches to a femoral neck and stem, which anchors in the femur (thigh) bone (see Fig. 1(b)). The femoral head articulates with an acetabular liner, which sits in an acetabular shell that is implanted in the pelvis. The articulation between the femoral head and acetabular liner/shell replaces the natural hip joint motion [4].

Prosthetic hip implant bearing surfaces exist with different material pairs, including metal-on-polyethylene (MoP), metal-on-metal (MoM), ceramic-on-polyethylene (CoP), and ceramic-on-ceramic (CoC). The hard-on-soft (MoP, CoP) material pairs are the most common due to their high fracture toughness and long-time clinical success [5]. Hard-on-hard material pairs exhibit lower in-vitro wear rates than hard-on-soft material pairs [6] but are prone to well-known problems such as metal ion release in MoM material pairs [7] and fracture [8] or squeaking [9] in CoC material pairs. In 2014, approximately 51% of new prosthetic hip implants in the US were CoP, 42% MoP, 4% MoM, and 3% CoC [10].

It is well-documented that the statistical survivorship of prosthetic hip implants declines significantly after 15–25 years of use [11]. A revision surgery replaces a failed prosthetic hip implant with a new one, which is risky for the patient and costly for the healthcare system. Thus, extending the longevity of prosthetic hip implants is of crucial importance. More than 47,000 THR revision surgeries occur in the US each year [12], which represents approximately 15% of all THR surgeries [13]. According to the NIS, the most common reasons for prosthetic hip implant failure include mechanical complications (19%), dislocation (17%), mechanical loosening (15%), and infection (14%) [12]. The literature documents that mechanical complications, instability, and loosening often find their origin in osteolysis caused by polyethylene wear debris from the acetabular liner [14]. Osteolysis is a condition in which the body's inflammatory response to foreign material, such as polyethylene wear debris from the acetabular liner, locally increases the rate of bone resorption and decreases the rate of bone reformation, resulting in weakening and loss of the bone around a prosthetic hip implant [15]. For that reason, reducing polyethylene wear remains critical to increasing the longevity and stability of prosthetic hip implants.

With increasingly younger patients receiving THR surgery [2] and, simultaneously, their life expectancy generally increasing [16], the fraction of THR patients that will outlive their prosthetic hip implant will increase with time. Thus, the number of revision surgeries will increase accordingly. As such, reducing the number of revision surgeries to improve patient quality of life and decrease healthcare costs represents a challenge for the orthopedic community.

Conventional methods to reduce polyethylene wear include improving material properties and bearing surface design. Increasing the degree of cross-linking in ultra-high molecular weight polyethylene (UHMWPE) increases strength and rigidity and decreases wear [17]. However, it may also increase oxidation, which reduces fracture and fatigue resistance, thus potentially increasing wear [18]. Anti-oxidant additives such as vitamin-E scavenger free radicals to limit oxidation of highly cross-linked

<sup>1</sup>Corresponding author.

Contributed by the Tribology Division of ASME for publication in the JOURNAL OF TRIBOLOGY. Manuscript received July 3, 2020; final manuscript received September 4, 2020; published online October 5, 2020. Assoc. Editor: Yi Zhu.

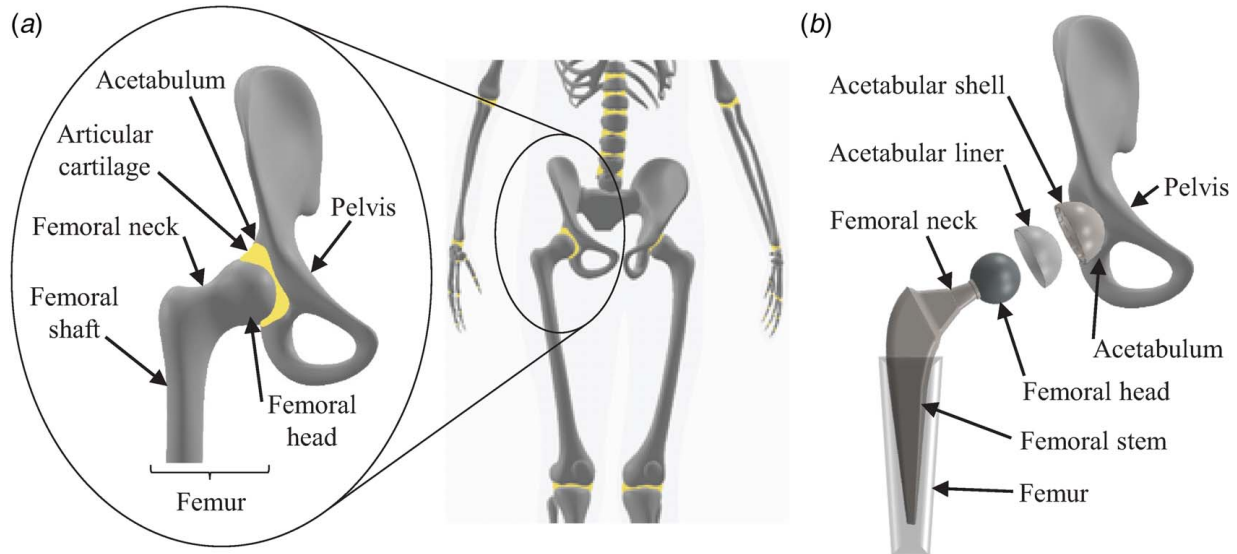


Fig. 1 Schematic of (a) the human hip and (b) a typical prosthetic hip implant. Modified from Ref. [3].

UHMWPE (HXLPE) [19]. As such, vitamin-E infused or blended cross-linked polyethylene (VEXPE) exhibits significantly lower wear and higher oxidation resistance than traditional UHMWPE material, which has been documented both in-vitro [20] and in-vivo [21].

Alternatively, changing the bearing surface design by replacing traditional cobalt-chromium-molybdenum (CoCrMo) femoral heads with advanced ceramic materials, or coating them with materials such as diamond-like carbon (DLC) [22], tantalum [23], or titanium nitride [24] increases the hardness and decreases the surface roughness of the femoral heads, thereby reducing polyethylene wear of the acetabular liner with which it articulates [25].

The literature documents that texture features on bearing surfaces can improve lubrication to reduce friction and wear in a variety of engineering applications [26,27]. Here, we consider only texture features on the bearing surfaces of orthopedic biomaterials to potentially reduce the friction coefficient and wear in prosthetic hip implants. We have searched the open literature on textured orthopedic biomaterial surfaces using combinations of search terms such as “surface texture,” “surface dimple,” “surface pattern,” “UHMWPE,” “CoCrMo,” “ceramic,” “hip implant,” and “knee implant” to find all publications that document man-made texture features on the bearing surfaces of orthopedic biomaterials. Figure 2 shows the number of publications in this area of research as a function of their publication year, categorized into experimental (blue), numerical simulations (red), and combined simulation and experimental (green) studies, showing increasing research activity since 2010. In addition, several patents have been issued on textured prosthetic implants.

Despite the promising results documented in many of these studies, no commercial prosthetic hip implants with textured bearing surfaces exist. Textured prosthetic hip implants will need to showcase substantially equivalent or improved safety and effectiveness compared to commercially available prosthetic hip implants in order to receive regulatory approval. The objective of this paper is to provide a comprehensive review and analysis of the existing literature on textured bearing surfaces in prosthetic hip implants, summarizing the state-of-the-art and discussing areas of opportunity to enable in-vivo textured prosthetic hip implants in the future.

## 2 Surface Texture Features

**2.1 Texture Feature Geometry and Functionality.** Figure 3 shows a three-dimensional view of a textured bearing surface. We identify all parameters that describe the geometry of the texture

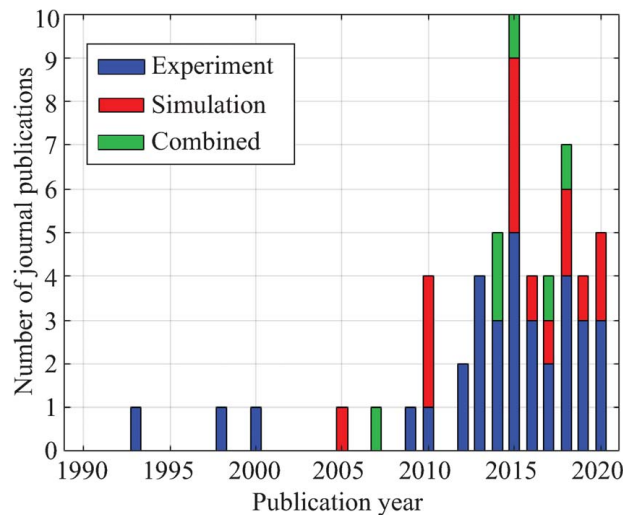
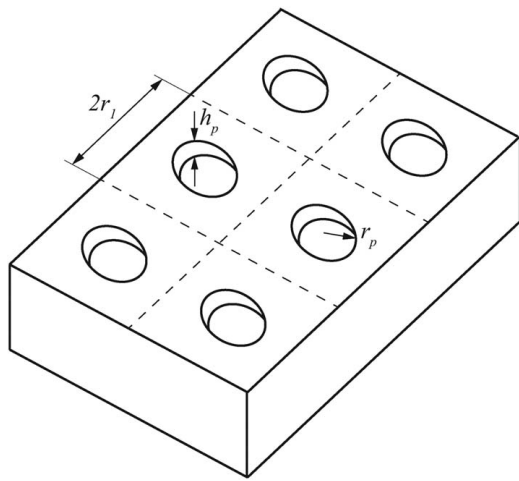


Fig. 2 The number of journal publications on the topic of textured orthopedic biomaterials as a function of publication year, categorized into experiments, simulations, and combined simulation and experiment

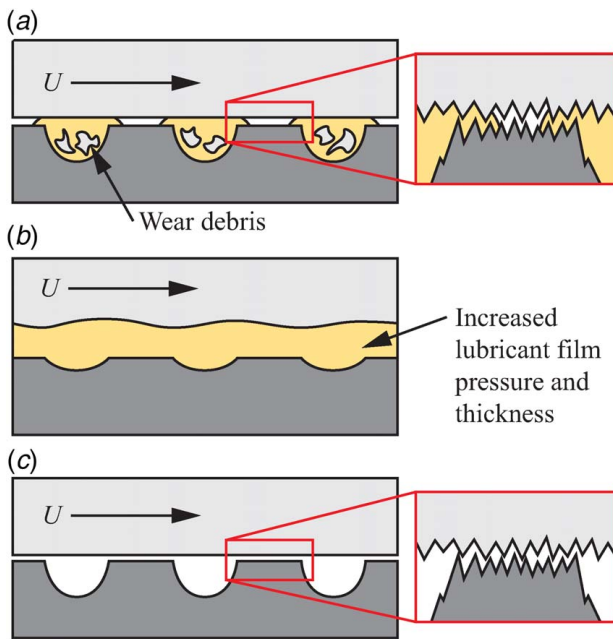
features and texture pattern. The texture aspect ratio is the ratio of the depth  $h_p$  and equivalent diameter  $2r_p$  of the texture feature, i.e.,  $\varepsilon = h_p/2r_p$ . The texture density is the ratio of the textured area to the entire bearing surface area. For instance, for a circular texture shape  $S_p = \pi r_p^2/4r_1^2$ , with  $2r_1$  the size of an imaginary square unit cell centered around the texture feature. The texture shape describes the two-dimensional contour of the texture feature on the bearing surface, whereas the texture floor profile describes the three-dimensional depth of the texture feature.

Figure 4 shows a cross-sectional view of a hard-on-soft textured bearing, where the bearing surfaces slide relative to each other with velocity  $U$ . It schematically illustrates the three functions that texture features can perform [26], depending on their geometry and the bearing operating conditions, each of which potentially contributing to reducing wear. In general, deep texture features ( $\varepsilon > 0.1$ ) function as lubricant reservoirs to reduce friction and wear under boundary or mixed lubrication conditions through a so-called secondary lubrication effect [28] by reserving and supplying lubricant to the bearing surfaces under starvation conditions (Fig. 4(a)). Additionally, they accumulate wear debris within the texture



**Fig. 3 Three-dimensional view of a textured bearing surface showing the geometry of the texture features**

features, thus reducing abrasive wear caused by third-body wear particles. We note that in extreme starvation conditions, deep texture features may reserve lubricant away from the contact area and, thus, have a negative impact on lubrication [29] and that accumulating wear debris away from the contact area may increase adhesive friction and wear under high loading conditions described in Ref. [30]. In contrast, shallow texture features ( $\epsilon < 0.1$ ) function as micro-hydrodynamic bearings that increase the lubricant film pressure and, correspondingly, the lubricant film thickness between both bearing surfaces for constant bearing load-carrying capacity. Increasing the lubricant film thickness, in turn, reduces contact between the bearing surfaces, which again reduces friction and wear (Fig. 4(b)). Partial texturing the inlet of a bearing surface produces greater lubricant film pressure than texturing the entire bearing surface [31,32]. A similar benefit is observed for partial texturing of the inlet and outlet of a bearing surface in reciprocating



**Fig. 4 Cross-sectional view of a textured hard-on-soft bearing, schematically illustrating the different possible functions of a textured bearing depending on texture geometry: (a) lubricant reservoirs and accumulating wear debris, (b) micro-hydrodynamic bearings, and (c) reducing the nominal contact area**

motion [33]. However, partial texturing has not yet been applied to prosthetic hip implants because the inlet/outlet of a sphere rotating in three dimensions is difficult to define. Finally, texture features also reduce the nominal contact area between bearing surfaces if contact occurs under boundary lubrication conditions (Fig. 4(c)).

Surface roughness affects cellular adhesion on the surface of prosthetic implant materials [34]. Qin et al. showed that surface texturing also has a significant effect on the adhesion, spreading, and proliferation of cells on the surface of orthopedic biomaterials [35]. This may impact the formation of biological films on the bearing surfaces of prosthetic hip implants, which has been shown to reduce the friction coefficient and wear of orthopedic biomaterials [36]. The effect of surface texturing on biological lubricant film formation should be studied in the future.

Figure 5(a) shows the texture aspect ratio versus the sliding parameter,  $S = \mu U/W$ , with  $\mu$  the dynamic viscosity of the lubricant,  $U$  the sliding velocity between both bearing surfaces, and  $W$  the bearing load-carrying capacity. This shows the texture design parameters and bearing operating conditions used by researchers

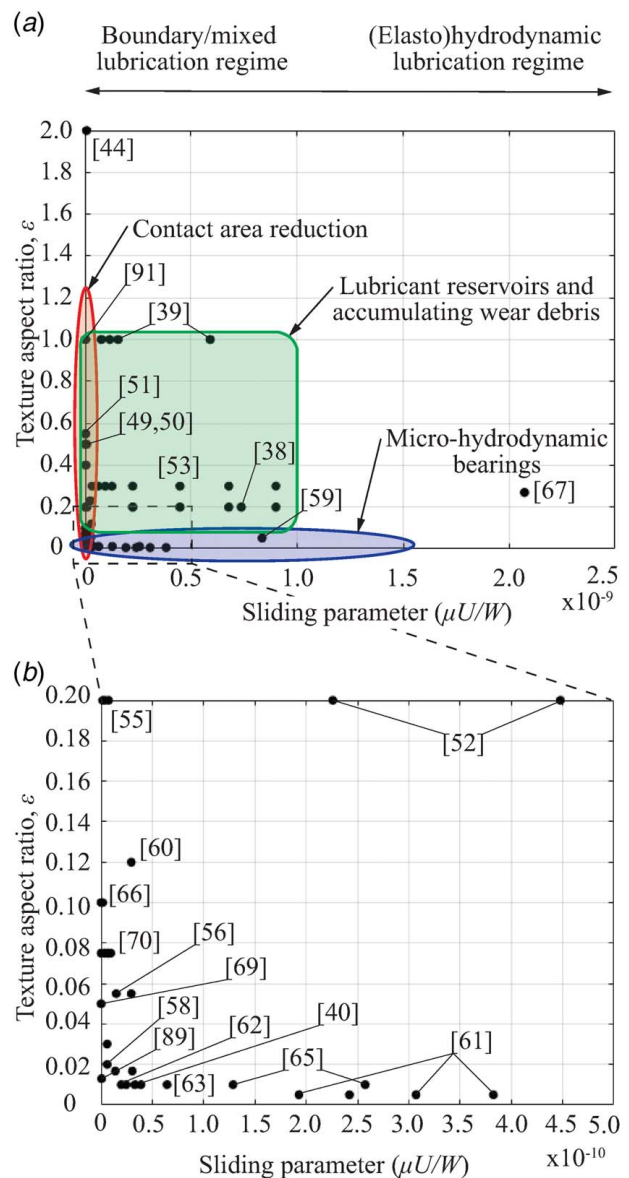


**Fig. 5 (a) Texture aspect ratio versus sliding parameter, identifying different lubrication regimes and showing individual studies as one or more black circle(s), grouping the studies based on texture function, and (b) close-up view.**

in the literature. We report each study in the open literature that documented reduced friction or wear for textured orthopedic biomaterial surfaces, and for which we could calculate a sliding parameter as one or more black circle(s), and identify the circles with the reference number of the study. We group the different studies based on the texture function (lubricant reservoirs and accumulating wear in green, micro-hydrodynamic bearings in blue, and contact area reduction in red), and link the sliding parameter to different lubrication regimes. Figure 5(b) shows a close-up view of the region with a small texture aspect ratio and small sliding parameter because many data points cluster here. We observe from Fig. 5 that texture features that function as lubricant reservoirs and accumulate wear debris display large texture aspect ratios ( $\epsilon > 0.1$ ), as they need physical space to accommodate lubricant and wear debris. Texture features that function as micro-hydrodynamic bearings require small texture aspect ratios ( $\epsilon < 0.1$ ) to increase the lubricant film pressure. The texture aspect ratio is not crucial to reduce the contact area, which is determined by the texture density. Further, this function is only relevant in the boundary lubrication regime when the bearing surfaces are in contact. In the following subsections, we review the research related to textured orthopedic biomaterials in the open literature, organized by texture function rather than chronological history, with the goal of using textured bearing surfaces in prosthetic hip implants.

We distinguish between experiments and numerical simulations, as both approaches have merits and limitations. Experiments attempt to recreate the physical operating conditions of a prosthetic hip implant but are limited by simplifications in geometry, kinematics, and loading. Numerical simulations enable fast and inexpensive evaluation of texture design parameters, but may not account for all physical mechanisms that occur in reality. We note the conditions used by each study in this review to qualify the results. Many studies report “optimum” results that may be misleading due to an incomplete dataset, or due to constraining a specific texture parameter. To find the global optimum, a full parametric study should be performed, as discussed in Ref. [37].

## 2.2 Lubricant Reservoirs and Accumulating Wear Debris.

Texture features that serve as lubricant reservoirs or to accumulate wear debris have been studied primarily through experiments with different texture designs, spatial configurations, and bearing operating conditions. For example, pendulum hip joint simulators (HJS) use the actual prosthetic hip implant geometries (spherical femoral head articulating with a hemispherical acetabular shell/liner) with a constant load and simplified kinematics restricted to a single plane. Some studies have textured the hard femoral head (Fig. 6(a)), and some have textured the soft acetabular liner (Fig. 6(b)). Researchers have demonstrated reduced friction coefficients and wear for both texture configurations, compared to smooth bearing surfaces.

Ito et al. first performed a pendulum HJS experiment with a textured CoCrMo femoral head and a UHMWPE acetabular liner, and observed that a textured compared to a smooth femoral head reduced the friction coefficient up to 36% and wear up to 69% and that UHMWPE wear debris accumulated in the texture features on the femoral head [38]. They attributed the reduced friction coefficient and wear to both the texture features dispensing lubricant to the bearing surfaces, and the texture features accumulating wear debris that otherwise might cause third-body adhesive or abrasive wear. Sagbas and Durakbasa performed a similar experiment to Ito et al. but with the opposite texture configuration, i.e., a smooth CoCrMo femoral head and textured UHMWPE and VEXPE acetabular liners, and measured the temperature increase of the bearing surfaces rather than the friction coefficient and wear [39]. They found that the lubricant retained in the texture features on the polyethylene surface served as a heat sink to reduce the bearing surface temperature up to 19% compared to the smooth acetabular liners, and they also observed wear debris accumulated in the texture features. Nečas et al. evaluated smooth metal and

ceramic femoral heads articulating with textured UHMWPE acetabular liners and measured a friction coefficient reduction of up to 40% with the textured as opposed to the smooth acetabular liners, which they attributed to the lubricant retained in the texture features [41]. Choudhury et al. used a pendulum HJS to measure the friction coefficient between textured and DLC-coated stainless steel femoral heads, articulating with ceramic acetabular liners. They found that a smooth DLC coating initially reduced the friction coefficient more than a combined textured and coated femoral head [42], but that the textured and coated femoral head maintained a constant friction coefficient over 10 repeated tests (approximately 450 cycles in 900 s), in contrast to the friction coefficient increasing by almost 24% during the same time interval for a smooth coated femoral head [43]. They attributed this observation to accumulating wear debris in the texture features, whereas the wear debris increased the friction coefficient between the smooth surfaces.

Pin-on-disk (PoD) configurations are also commonly used to measure the friction coefficient and wear between small samples (pin and disk) of orthopedic biomaterials. They are faster and less expensive than HJS experiments and, thus, facilitate the screening of different material pairs and/or texture designs. Nishimura et al. performed PoD experiments with stainless steel pins articulating against textured UHMWPE disks, and with UHMWPE pins articulating against textured stainless steel disks [44]. They determined the optimum texture aspect ratio and density as  $\epsilon = 2.00$  and  $S_p = 0.14$ , which reduced the friction coefficient by 25% and wear by 33%, respectively, compared to smooth bearing surfaces. They attributed these results to the texture features retaining lubricant and accumulating wear debris when the smooth surface experienced lubrication starvation and accelerated abrasion due to the wear debris. Young et al. used smooth hemispherical CoCrMo pins articulating with textured UHMWPE disks and measured that the friction coefficient reduced by 42% compared to a smooth disk, because the texture features supplied lubricant to the contact area and accumulated wear debris [45]. However, they also measured a 37% increase of wear compared to a smooth disk, which could be due to plastic deformation at the edges of the texture features. Sagbas and Durakbasa also used smooth CoCrMo pins articulating with textured UHMWPE and VEXPE disks and demonstrated that the friction coefficients decreased by approximately 29% and 22% and the corresponding wear volumes decreased by 39% and 60% compared to smooth UHMWPE and smooth VEXPE, respectively [46]. They attributed these results to the texture features functioning as lubricant reservoirs. Sawano et al. used smooth UHMWPE pins

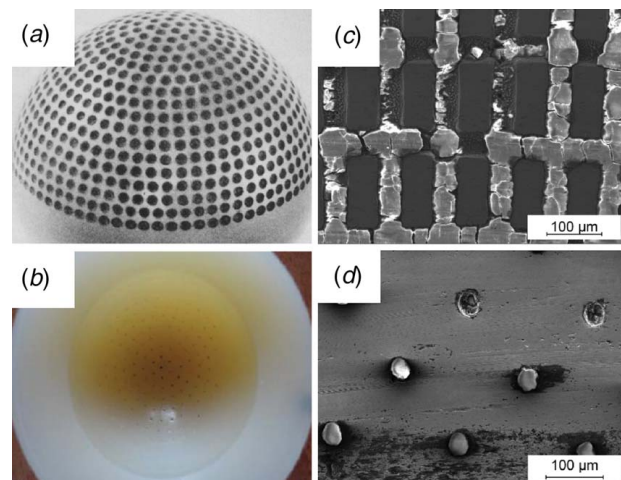


**Fig. 6 (a) Large texture features designed to function as lubricant reservoirs on the surface of a CoCrMo femoral head [38]. (b) Texture features are designed to function as lubricant reservoirs on the surface of a UHMWPE acetabular liner [39]. (c) CoCrMo wear debris trapped in groove texture features [40]. (d) CoCrMo wear debris trapped in spherical texture features [40].**

articulating with textured CoCrMo disks and determined that  $1\ \mu\text{m}$  was the optimum texture feature depth to accumulate wear debris because texture feature depths smaller than  $1\ \mu\text{m}$  could not accumulate enough wear debris to protect the surface from abrasive wear, and texture features deeper than  $1\ \mu\text{m}$  exhibited asperities between the texture features that scratched the UHMWPE surface [47]. Guo et al. applied a hydrogel to a textured bearing surface to promote the slow release of lubricant to the articulating surface of PoD experiments with smooth UHMWPE pins and textured CoCrMo disks and found the textured disks to reduce the friction coefficient by 57% compared to the untextured disks [48]. Pratap and Patra evaluated smooth titanium pins against textured titanium disks and showed that micro-groove texture features reduced the friction coefficient up to 34%, whereas spherical texture features reduced the friction coefficient up to 24% [49]. The micro-groove texture features led to a greater reduction of the friction coefficient because they reserved a greater volume of lubricant and showed greater wettability than the spherical texture features. Lee et al. used titanium pins articulating with textured and thermally oxidized titanium disks and reported a 57% friction coefficient reduction and a 99% wear reduction with a textured and oxidized surface compared to a smooth oxidized surface [50]. Oxidized surfaces display increased hardness compared to non-oxidized surfaces, which protected the texture features on the oxidized surfaces from wearing away and allowed the texture features to accumulate wear debris. Thus, this work also illustrates how surface treatments of the bearing surfaces might reduce wear and potentially render titanium suitable as a bearing material in prosthetic hip implants.

Other friction and wear measurement configurations include ball-on-disk (BoD), in which the kinematics may include rolling and sliding, and ring-on-disk (RoD), in which one bearing surface rotates around its center axis while sliding over the other bearing surface. López-Cervantes et al. used a smooth stainless steel ball and textured UHMWPE disk and measured a 14% reduction of the friction coefficient for the textured as opposed to a smooth UHMWPE disk, which they explained by the lubricant being squeezed from the texture features to areas of local lubrication starvation [51]. Similarly, Sufyan et al. performed BoD experiments using a smooth ceramic ball and a textured UHMWPE disk, and they measured up to a 44% and 42% friction coefficient and wear reduction, respectively, when using a square grid of groove texture features compared to a smooth UHMWPE surface [52]. They concluded that lubricant trapped in the groove texture features enhanced the lubricant film and decreased contact between the textured compared to the smooth bearing surfaces. Further, Zhang et al. performed RoD experiments using smooth stainless steel rings articulating with textured UHMWPE disks and found the optimum texture aspect ratio to increase with increasing bearing load-carrying capacity because larger texture features can dispense more lubricant to starved regions as the increased load-carrying capacity squeezes the lubricant from the texture features [53]. They also used textured stainless steel rings articulating with smooth UHMWPE disks to determine the optimum texture design parameters [54]. Their experiments demonstrated that both texture configurations reduced the friction coefficient at low bearing load-carrying capacity ( $W=0.24\ \text{MPa}$ ) but required a different texture density ( $S_p=0.10$  for the textured stainless steel surface and  $S_p=0.30$  for the textured UHMWPE surface). At high bearing load-carrying capacity ( $W=1.67\ \text{MPa}$ ), only the textured UHMWPE surface could reduce friction and wear because the texture features on the hard surface experience increased contact pressure at the edge of the texture features, which caused increased friction and abrasive wear. Wang et al. used textured stainless steel rings articulating with different polymer disks, including UHMWPE, and they determined that texture features on the hard surface increased the friction coefficient, but specific texture parameters ( $\epsilon=0.05$ ,  $S_p=0.20$ ) could reduce the wear-rate under the operating conditions they evaluated, likely because of wear debris accumulation [55]. Tarabolsi et al. performed RoD experiments of both CoCrMo and alumina-based material pairs with different texture patterns,

including grooves and spherical texture features [40]. They observed wear debris accumulating inside the texture features (see Figs. 6(c) and 6(d)), thus causing the wear volume to decrease by up to 87% compared to smooth surfaces.

In addition to experimental works, a few numerical simulations also provide important information to understand the different functions of texture features. Zhang et al. simulated texture features made of concentric rings on CoCrMo surfaces to visualize the lubricant being squeezed from the texture features to starved contact areas and validated the results with PoD experiments, showing a 31% reduction of the friction coefficient compared to smooth bearing surfaces [56].

Table 1 summarizes each paper included in this review that used texture features as lubricant reservoirs and to accumulate wear debris. This information includes the experiment configuration, operating conditions, and the corresponding friction coefficient and wear results. Note that most values in the table are reported with standard units and consistent significant digits. However, we have reported the wear measurements in the units and with the precision provided by each individual publication.

**2.3 Micro-Hydrodynamic Bearings.** Several publications also describe texture features specifically designed to function as micro-hydrodynamic bearings that increase the lubricant film pressure and, for constant bearing load-carrying capacity, the lubricant film thickness. Consequently, texture features that function as micro-hydrodynamic bearings could alter the lubrication regime of the bearing, depending on the texture design parameters and the bearing operating conditions. Figure 7(a) shows the local lubricant film pressure as a function of the length coordinate along the centerline of a typical spherical texture feature designed to function as a micro-hydrodynamic bearing. We show the floor profile along the centerline of the spherical texture feature for reference. The lubricant flow encounters a diverging geometry at the inlet, followed by a converging geometry at the outlet of the texture feature, which causes the lubricant film pressure to locally decrease and subsequently increase if the lubricant mass flow remains constant (steady-state). Repeated over many texture features, this increases the average lubricant film pressure and, correspondingly, either the lubricant film thickness for constant bearing load-carrying capacity or, alternatively, the bearing load-carrying capacity for constant lubricant film thickness. Figure 7(b) shows lubricant flow lines inside infinitely wide texture features with increasing texture aspect ratio to illustrate how a vortex forms at the bottom of texture features with increasing texture aspect ratio. Shallow texture features are most desirable to function as micro-hydrodynamic bearings because a vortex inside the texture feature effectively reduces the converging lubricant flow and, thus, reduces the increase in lubricant film pressure.

Interferometry has long been used to measure the lubricant film thickness [60]. Choudhury et al. performed pendulum HJS experiments with textured CoCrMo femoral heads and glass acetabular cups and used interferometry measurements to show that shallow texture features ( $\epsilon<0.03$ ) increased the lubricant film thickness almost 3.5 times compared to smooth femoral heads [61]. Dong et al. also performed pendulum HJS experiments with textured and carburized CoCrMo femoral heads articulating with glass acetabular liners [58] and similarly demonstrated that for shallow texture features ( $\epsilon<0.05$ ) the lubricant film thickness increased up to 560% and the friction coefficient decreased by 43% compared to using smooth CoCrMo femoral heads. Figure 7(c) shows interferometry images of the smooth (left) and textured (right) CoCrMo femoral heads, at the instances of minimum (top) and maximum (bottom) sliding velocity. The graph below shows the lubricant film thickness measured using interferometry, as a function of sliding distance corresponding to each image (1–4), showing that the lubricant film thickness increases because of the texture features functioning as micro-hydrodynamic bearings, modified from Ref. [58]. Another study by Choudhury et al. using pendulum HJS experiments found that textured CoCrMo femoral heads reduced the friction coefficient

**Table 1 Data summary of publications that describe using texture features as lubricant reservoirs and to accumulate wear debris**

Reference	Texture aspect ratio, $\epsilon$	Texture density, $S_p$	Experiment configuration	Lubricant	Load-carrying capacity [MPa]	Sliding velocity [m/s]	Friction coefficient (smooth)	Friction coefficient (textured)	Wear (smooth)	Wear (textured)
Ito et al. [38]	0.200	0.136	Pendulum HJS	Water	0.554–3.695	0.027–0.408	0.058–0.077	0.037–0.064	1.1–23.1 mg	0.7–7.2 mg
Sagbas and Durakbasa [39]	1.000	0.049	Pendulum HJS	Bovine serum	0.325–2.436	0.088	—	—	—	—
Nečas et al. [41]	0.017	0.150	Pendulum HJS	Model synovial fluid	3.600	0.050	0.096–0.422	0.077–0.380	—	—
Choudhury et al. [42]	0.230	0.049	Pendulum HJS	Bovine serum	3.565	0.039	0.084–0.119	0.107–0.121	—	—
Choudhury et al. [43]	0.230	0.049	Pendulum HJS	Bovine serum	3.565	0.039	0.104	0.107	—	—
Nishimura et al. [44]	1.000–5.000	0.049–0.545	PoD	Saline	12.369–N/A	N/A	0.005	0.003	12 $\mu\text{m}$	8 $\mu\text{m}$
Young et al. [45]	2.000	0.087	PoD	Bovine serum	30.000	0.110	0.060	0.035	0.791 $\text{mm}^3$	1.251 $\text{mm}^3$
Sagbas and Durakbasa [46]	1.000	0.049	PoD	Water	N/A	N/A	0.090–0.170	0.070–0.120	$3.38 \times 10^{-5}$ – $4.54 \times 10^{-5}$ $\text{mm}^3/\text{Nm}$	$1.34 \times 10^{-5}$ – $2.75 \times 10^{-5}$ $\text{mm}^3/\text{Nm}$
Sawano et al. [47]	N/A	N/A	PoD	Water	5.200	0.019	—	—	0.42 mg	0.18 mg
Gou et al. [48]	0.540	0.162–0.401	PoD	Bovine serum and hydrogel	3.600	0.010–0.017	0.100	0.043	—	—
Pratap and Patra [49]	0.115–0.210	0.066–0.918	PoD	Bovine serum	106.700–151.000	0.010–0.100	0.198–0.297	0.146–0.201	—	—
Lee et al. [50]	0.500	0.160	PoD	Bovine serum	5.000	0.015	0.610–0.670	0.290–0.800	130.0–255.0 mg	0.4–280.0 mg
López-Cervantez et al. [51]	0.500–1.000	0.649	BoD	Water	19.000–24.000	0.005–0.055	0.024–0.026	0.0221–0.0225	—	—
Sufyan et al. [52]	0.550	0.490	BoD	Bovine serum	12.200–26.680	0.012	0.018–0.180	0.019–0.090	12 $\mu\text{m}$	17 $\mu\text{m}$
Zhang et al. [53]	0.025–0.300	0.050–0.400	RoD	Water	0.239–1.670	0.054–0.215	0.045–0.120	0.015–0.020	2.5 $\mu\text{m}$	0.9 $\mu\text{m}$
Zhang et al. [54]	0.300	0.050–0.400	RoD	Water	0.239–1.670	0.054–0.215	0.050–0.120	0.010–0.190	2.5 $\mu\text{m}$	1.0 $\mu\text{m}$
Wang et al. [55]	0.025–0.050	0.100–0.400	RoD	Water	0.150–0.250	0.440	0.100	0.120–0.250	0.0175 $\text{mm}^3/\text{Nm}$	0.0090 $\text{mm}^3/\text{Nm}$
Tarabolsi et al. [40]	0.200–0.400	0.087–0.660	RoD	Bovine serum, water	9.000	0.015	0.290–0.700	0.240–0.400	0.03–0.40 $\text{mm}^3$	0.02–0.16 $\text{mm}^3$
Zhang et al. [56]	0.055	0.283	PoD/mixed simulation	Bovine serum	3.500	0.024	0.233	0.160	—	—

Note: The wear results are reported in the units and precision provided by each individual study.

by 31% and increased the lubricant film thickness 133% when articulating with CoCrMo acetabular liners, i.e., an MoM material pair. However, they measured an increase of the friction coefficient by 24% when articulating with HXLPE acetabular liners, i.e., an MoP material pair [62]. They explained this observation as the soft polyethylene surfaces deforming and penetrating into the texture features on the hard femoral head.

Chyr et al. [63] and Qiu et al. [64] built and used a hybrid testing apparatus comprising a textured CoCrMo cylinder that articulates with smooth UHMWPE specimens and validated their numerical simulations that showed that shallow texture features ( $\epsilon < 0.1$ ) reduce the friction coefficient by increasing the lubricant film pressure and thickness under constant bearing load-carrying capacity.

Borjali et al. [65] and Langhorn et al. [66] performed unidirectional and multi-directional PoD wear experiments of UHMWPE, HXLPE, and VEXPE pins articulating with textured and smooth CoCrMo disks and showed that the textured CoCrMo disks reduced the wear-rate of all UHMWPE, HXLPE, and VEXPE pin materials, compared to smooth CoCrMo disks. Borjali et al. also showed that the texture features reduced the friction coefficient compared to smooth CoCrMo disks and transitioned the bearing from operating in the boundary or mixed lubrication to the full-film (elasto)hydrodynamic lubrication regime [67]. Others have also documented that texture features may transition the bearing from operating in the boundary or mixed lubrication regimes to the full-film regime, including Dougherty et al. who used a stainless steel pin articulating with a textured UHMWPE disk [68], and Cho and Choi who used a

UHMWPE pin articulating with a textured stainless steel disk [59]. Figure 7(d) shows a Stribeck curve (friction coefficient versus Sommerfeld number) obtained by Cho and Choi [59], which illustrates how a textured bearing (open triangle markers) reduces the friction coefficient such that it operates in the (elasto)hydrodynamic lubrication regime where the equivalent smooth bearing (solid square markers) operates in the boundary and mixed lubrication regimes, for the same operating conditions. Kashyap and Ramkumar also used PoD experiments with smooth UHMWPE pins and titanium disks textured with cross-hatched groove patterns and found an optimum groove aspect ratio ( $\epsilon = 0.050\text{--}0.066$ ) that reduced the friction coefficient by 13% and wear by 58%, which they attributed to an increased lubricant film pressure and thickness compared to an untextured bearing [69]. Roy et al. performed PoD friction experiments using a ceramic pin articulating with a textured and smooth ceramic disk and determined that the friction coefficient decreased by 17% and wear decreased by 53% for the textured compared to the smooth ceramic disks [70,71], which they attributed to the increased lubricant film pressure in the textured bearing.

In addition to increasing the lubricant film pressure and thickness, texture features that function as micro-hydrodynamic bearings may also increase the lubricant viscosity in non-Newtonian lubricants because joint lubricants exhibit shear-thinning behavior, i.e., their viscosity decreases with increasing shear rate. Drescher et al. used RoD experiments of smooth CoCrMo rings and textured CoCrMo disks lubricated with the bovine serum to show that texture features locally increase the spacing between bearing surfaces, which

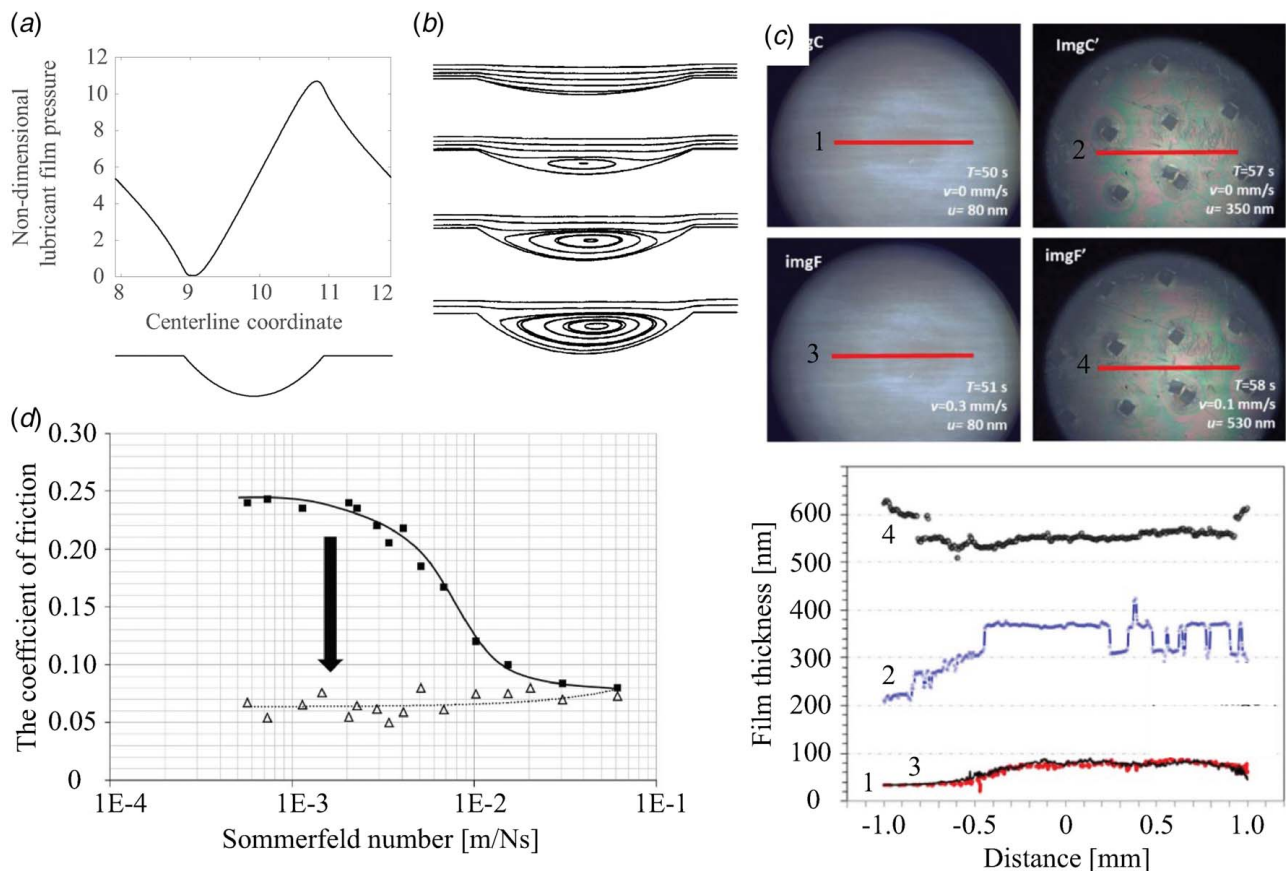


**Fig. 7** (a) The local lubricant film pressure as a function of the length coordinate along the centerline of a typical spherical texture feature with the texture floor profile below. (b) Lubricant flow lines inside infinitely wide texture features, showing increasing vortex formation with increasing texture aspect ratio [57]. (c) Interferometry images of smooth (left) and textured (right) CoCrMo femoral heads at the minimum (top) and maximum (bottom) sliding velocity, with the measured lubricant film thickness below as a function of sliding distance for each femoral head, modified from [58]. (d) Stribeck curves (friction coefficient versus Sommerfeld number) showing the transition in the lubrication regime for textured (open triangle markers) compared to smooth (solid square markers) surfaces [59].

decreases the local shear rate and increases the local viscosity [72,73]. They found that the textured disks increased the lubricant viscosity up to 40% compared to a smooth disk. Increasing the lubricant viscosity will also increase the lubricant film pressure when all other operating and design parameters remain constant.

However, not all texture parameters reduce the friction coefficient and wear of the bearing materials. Few reports document an increase of the friction coefficient and wear-rate of textured bearing surfaces compared to smooth ones. For instance, Zhou et al. used PoD experiments with UHMWPE pins articulating with stainless steel disks with shallow texture features, but reported an increase of the friction coefficient and wear rate compared to smooth stainless steel disks, which they attributed to the build-up of material around the contour of the texture features that resulted from manufacturing the texture features [74].

Numerical simulations have also provided insight into how texture features may function as micro-hydrodynamic bearings, and they have been widely used to optimize the texture design parameters in terms of, e.g., minimizing the friction coefficient or maximizing the lubricant film thickness. Computational fluid dynamics (CFD) solve the Navier-Stokes (N-S) equations to simulate the lubricant film pressure and thickness between two bearing surfaces in relative motion. Sahlin et al. [57] and Han et al. [75] performed CFD simulations of lubricant films between a smooth and a textured rigid surface in two and three dimensions, respectively. They simulated a wide range of lubricants and bearing operating conditions and determined optimum texture aspect ratios that maximize the load-carrying capacity of the lubricant film under different operating conditions. Sahlin et al. showed that vortex formation increases with increasing texture aspect ratio, for constant bearing operating conditions (see Fig. 7(b)).

However, solving the full N-S equations is computationally expensive and is often not needed to solve lubrication problems because the lubricant film thickness separating the bearing surfaces is much smaller than the length scale of the bearing surfaces. Instead, the Reynolds equation (RE), which represents a reduced version of the N-S equations based on thin-film assumptions such as constant pressure and viscosity through the lubricant film thickness, velocity gradient perpendicular to the lubricant film thickness, negligible inertial effects, laminar flow, and Newtonian lubricant behavior, can accurately simulate the lubricant film pressure and thickness in textured bearings [76]. Specifically, Qiu et al. evaluated each assumption implicit to the RE and determined where each assumption breaks down in textured bearings by comparing the solutions of the RE to those of the full N-S equations [77].

Rahmani and Rahnejat solved the RE in two-dimensional hydrodynamic lubrication (HL) model of a non-dimensional lubricant film between a smooth and a textured rigid surface to investigate flat and sloped texture floor profiles of infinitely wide textured bearings. They found that the optimum depth of the texture features is proportional to the lubricant film thickness, but depends on the texture floor profile because the different texture floor profiles cause the lubricant film to locally diverge/converge at different rates [78]. Qiu and Raeymaekers used HL simulations to evaluate the effect of surface roughness inside the texture features on a rigid bearing surface and found that repeating sinusoidal roughness increased the bearing load-carrying capacity, but random roughness inside the texture features had a negligible effect [79]. Zhang et al. also performed HL simulations of a CoCrMo pin articulating with a textured UHMWPE disk with different texture feature shapes to maximize the lubricant film thickness and minimize the friction coefficient [80]. They found that square-shaped texture features with  $\varepsilon=0.07$  and  $S_p=0.20$  reduced the friction coefficient more than 18% compared to circular-shaped texture features. Additionally, Shen and Khonsari numerically optimized the texture feature shape, unbound to any geometry, to maximize the lubricant film pressure and bearing load-carrying capacity under HL conditions [81]. They found that the optimized texture feature shapes increased the bearing load-carrying capacity compared to standard texture feature shapes such as circles or squares.

The previous paragraph gives an overview of research in which the bearing surfaces were considered rigid, i.e., their compressibility is much smaller than that of the lubricant. However, this assumption is not valid in the case of e.g., an MoP or CoP prosthetic hip implant where the polyethylene bearing surface may deform under the lubricant film pressure and, thus, one must account for this deformation. Su et al. used an elasto-hydrodynamic lubrication (EHL) model of a textured UHMWPE surface articulating with a smooth steel surface by simultaneously computing the lubricant film pressure using the RE and solving the elasticity equations to compute the deformation of the soft UHMWPE surface [82]. They found that the optimum texture parameters ( $\varepsilon$  and  $S_p$ ) to maximize the bearing load-carrying capacity both increase compared to HL simulations. Allen and Raeymaekers used an EHL model of textured CoCrMo articulating with smooth UHMWPE to determine the optimum texture design parameters that maximize the lubricant film thickness for a range of bearing operating conditions [83]. They found that the optimum texture aspect ratio varies with the bearing operating conditions such that it is proportional to the lubricant film thickness, and the stiffness of the UHMWPE surface does not affect the lubricant film thickness. Allen and Raeymaekers also showed that flat texture floor profiles produce thicker lubricant films than round or sloped texture floor profiles and observed that the volume of the texture features is directly proportional to the lubricant film thickness, independent of the texture floor profile [84].

During in-vivo gait, prosthetic hip implants may operate in the boundary or mixed lubrication regimes for a portion of the gait cycle during which either the load is high or the relative velocity between the bearing surfaces is small. That portion of the gait cycle cannot be modeled by HL or EHL models that require full-film lubrication with no solid-on-solid contact. However, mixed lubrication models combine simultaneous computations of fluid lubrication and solid asperity contact to account for solid-on-solid contact. For instance, Basri et al. used a fluid–solid interaction (FSI) model in a multi-physics computational framework to show that texture features increase the lubricant film pressure and thickness, thus decreasing the solid-on-solid contact in an MoM prosthetic hip implant [85]. Gao et al. used a mixed lubrication model of a MoM prosthetic hip implant with texture features on both the femoral head and acetabular liner with dynamic operating conditions of a human gait cycle. They found that the texture features reduced contact between the bearing surfaces during approximately 80% of the gait cycle (particularly in the boundary and mixed lubrication regimes), but the texture features slightly decreased the lubricant film thickness compared to smooth bearing surfaces when the bearing already operated in the full-film lubrication regime [86]. This shows that the texture features improve the lubricant film thickness during the portion of the gait cycle where it will have the greatest impact on reducing wear. Gao et al. also modeled a CoCrMo MoM prosthetic hip implant with a textured, spherical femoral head and an aspherical acetabular liner under dynamic operating conditions, and found the texture to slightly decrease the film thickness for the geometry and operating conditions considered in their work [87]. Gao et al. also established a mixed lubrication model of an MoP prosthetic knee implant with a rigid, smooth femoral component and deformable, textured UHMWPE tibial insert [88]. They found that texture features could increase the lubricant film thickness and reduce wear by 4% in the lateral compartment of the prosthetic knee implant, but that texture features slightly decreased the lubricant film thickness and increased the wear in the medial compartment of the prosthetic knee implant because of the medial compartment experiences higher loads than the lateral compartment.

Table 2 summarizes each paper included in this review which used texture features as micro-hydrodynamic bearings. Note that most values in the table are reported with standard units and consistent significant digits. However, we have reported the wear measurements in the units and with the precision provided by each individual publication.

**Table 2 Data summary of publications that describe using texture features as micro-hydrodynamic bearings**

Reference	Texture aspect ratio, $\varepsilon$	Texture density, $S_p$	Experiment configuration	Lubricant	Load-carrying capacity [MPa]	Sliding velocity [m/s]	Friction coefficient (smooth)	Friction coefficient (textured)	Wear (smooth)	Wear (textured)
Choudhury et al. [61]	0.020–0.030	0.170–0.250	Pendulum HJS	Bovine serum	16.000	0.044	—	—	—	—
Dong et al. [58]	0.027–0.050	0.370–0.580	Pendulum HJS	Bovine serum	0.081	0.031	0.190–0.300	0.150–0.170	—	—
Choudhury et al. [62]	0.055–0.120	0.150	Pendulum HJS	Bovine serum	3.245	0.044	0.140–0.160	0.110–0.170	—	—
Chyr et al. [63]	0.005–0.020	0.050–0.200	Hybrid tester	Bovine serum	0.570–1.130	0.100	0.260–0.280	0.120–0.290	—	—
Qiu et al. [64]	0.010–0.020	0.050–0.200	Hybrid tester	Bovine serum	5.600–11.100	0.100	0.200	0.100	—	—
Borjali et al. [65]	0.010–0.040	0.050–0.300	PoD	Bovine serum	2.000	0.031	—	—	1.3–5.4 mg/M cycles	0.6–2.6 mg/M cycles
Langhorn et al. [66]	0.005–0.020	0.050–0.200	PoD	Bovine serum	Dynamic	0.038	—	—	6.83 mg/M cycles	2.18 mg/M cycles
Borjali et al. [67]	0.010–0.040	0.050–0.300	PoD	Bovine serum	1.000–2.000	0.031–0.063	0.070–0.090	0.050–0.075	—	—
Dougherty et al. [68]	0.100	0.030–0.500	PoD	Water	44.360–60.100	0.005–0.070	0.075	0.040	—	—
Cho and Choi [59]	0.270–1.000	0.050–0.250	PoD	Oil	2.500	0.100	0.262	0.092	—	—
Kashyap and Ramkumar [69]	0.040–0.200	0.100–0.400	PoD	Bovine serum	8.620–15.527	0.020	0.367–0.414	0.319–0.441	0.90–1.27 mg	0.38–2.92 mg
Roy et al. [70]	0.050	0.058	PoD	Bovine serum	132.000–187.000	0.010	0.165–0.182	0.14–0.176	—	—
Roy et al. [71]	0.075–0.100	0.050–0.150	PoD	Bovine serum	181.450–256.610	0.020–0.080	0.132–0.150	0.108–0.125	0.77 mg	0.36 mg
Dresher et al. [72]	0.020–2.000	0.031–0.278	RoD	Bovine serum	—	0.010	—	—	—	—
Dresher et al. [73]	0.330–1.330	0.026–0.105	RoD	Bovine serum	—	0.010	—	—	—	—
Zhou et al. [74]	0.003	0.049	PoD	Bovine serum	1.600	N/A	—	—	$2.25 \times 10^{-7}$ – $2.47 \times 10^{-7}$ mm <sup>3</sup> /Nm	$2.64 \times 10^{-7}$ – $2.93 \times 10^{-7}$ mm <sup>3</sup> /Nm
Sahlin et al. [57]	0.015–0.250	0.150–0.500	HL simulation	Non-dimensional	—	Non-dimensional	3.000	2.770	—	—
Han et al. [75]	N/A	0.031–0.503	HL simulation	Non-dimensional	—	Non-dimensional	N/A	0.500–5.400	—	—
Rahmani and Rahnejat [78]	N/A	N/A	HL simulation	Non-dimensional	N/A	N/A	1.000	0.852–0.884	—	—
Qiu and Raeymaekers [79]	0.010	0.200	HL simulation	Non-dimensional	—	10.000	—	—	—	—
Zhang et al. [80]	0.120–0.600	0.040–0.400	HL simulation	Non-dimensional	N/A	N/A	N/A	1.010–1.280	—	—
Shen and Khonsari [81]	N/A	0.100–0.300	HL simulation	Non-dimensional	—	0.010–5.120	—	—	—	—
Su et al. [82]	0.002–0.010	0.100–0.500	EHL simulation	Paraffin oil	—	1.200	—	—	—	—
Allen and Raeymaekers [83]	0.010–0.100	0.100–0.700	EHL simulation	Non-dimensional	0.250–2.000	Non-dimensional	—	—	—	—

Table 2 Continued

Reference	Texture aspect ratio, $\epsilon$	Texture density, $S_p$	Experiment configuration	Lubricant	Load-carrying capacity [MPa]	Sliding velocity [m/s]	Friction coefficient (smooth)	Friction coefficient (textured)	Wear (smooth)	Wear (textured)
Allen and Raeymaekers [84]	0.010–0.100	0.100–0.700	EHL simulation	Non-dimensional	0.250–2,000	Non-dimensional	—	—	—	—
Basri et al. [85]	0.250	0.070–0.280	Mixed lubrication simulation	Synovial fluid	Dynamic	Dynamic	—	—	—	—
Gao et al. [86]	0.003	0.031	Mixed lubrication simulation	Synovial fluid	Dynamic	Dynamic	—	—	—	—
Gao et al. [87]	0.003	0.031	Mixed lubrication simulation	Synovial fluid	Dynamic	Dynamic	—	—	—	—
Gao et al. [88]	0.250–1.667	0.098–0.503	Mixed lubrication simulation	Synovial fluid	Dynamic	Dynamic	—	—	2.19–4.68 mm <sup>3</sup>	—

Note: Wear measurements are reported with the units and precision given by each journal publication.

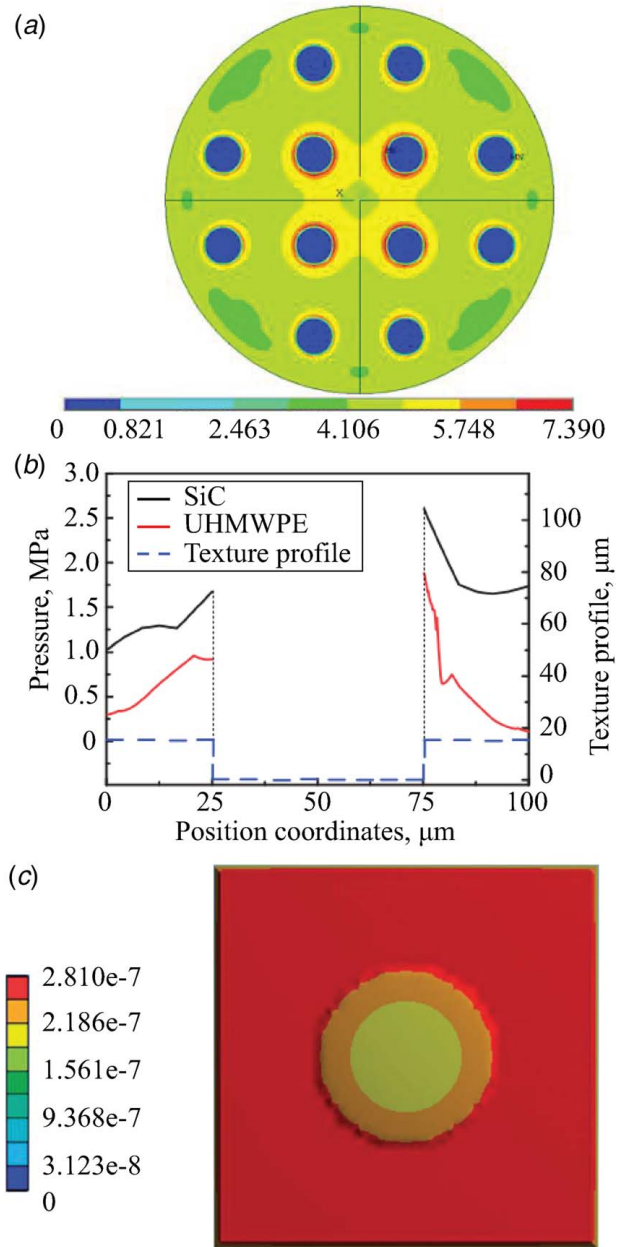


Fig. 8 (a) FEA showing the contact pressure (in MPa) on a textured CoCrMo surface with  $\epsilon=0.28$  and  $S_p=0.13$  in contact with a UHMWPE surface [93]. (b) Contact pressure along the centerline and near the edge of a texture feature for stiff SiC and soft UHMWPE [94]. (c) Deformation of a smooth UHMWPE surface (in m) in contact with a textured stainless steel surface [94].

**2.4 Reducing the Nominal Contact Area Between the Bearing Surfaces.** Texture features also reduce the nominal contact area between both bearing surfaces in contact, independent of the texture aspect ratio, and entirely driven by the texture density. Several experiments have investigated how a reduction of the nominal contact area in textured bearings may change their friction coefficient or wear-rate. Such experiments are typically performed “dry,” i.e., without lubricant, to entirely isolate the function of contact area reduction by avoiding that the texture features function as lubricant reservoirs or micro-hydrodynamic bearings.

Cuervo et al. used PoD experiments of a titanium pin with raised elliptical texture features (to mimic the texture of snakeskin scales) articulating with smooth UHMWPE disks. They demonstrated that the friction coefficient of the textured pin against the UHMWPE

**Table 3 Data summary of publications that describe using texture features to reduce the nominal contact area**

Reference	Texture aspect ratio, $\epsilon$	Texture density, $S_p$	Experiment configuration	Lubricant	Load-carrying capacity [MPa]	Sliding velocity [m/s]	Friction coefficient (smooth)	Friction coefficient (textured)	Wear (smooth)	Wear (textured)
Cuervo et al. [89]	0.011–0.037	0.230–0.300	PoD	—	16.330–28.350	1.000	0.140–0.200	0.060	—	—
Wei et al. [90]	—	—	BoD	—	179.536	$5.000 \times 10^{-4}$	0.330	0.120	—	—
Kustandi et al. [91]	1.000	0.500	BoD	—	300.000	0.010	0.300	0.180	—	—
Choudhury et al. [92]	0.067	0.045	PoD	Bovine serum	17.900–24.700	0.010	0.049–0.188	0.058–0.183	0.041–0.101 mg	0.061–0.130 mg
Pakhaliuk et al. [93]	0.050–0.500	0.002–0.785	Contact surface simulation	—	5.410–6.280	—	—	—	—	—
Wang et al. [94]	0.360	0.200	Contact surface simulation	—	1.670	$1.000 \times 10^{-4}$	—	—	—	—
Dong et al. [95]	N/A	N/A	Contact surface simulation, Pendulum HJS	Alcohol	0.124	0.017	—	—	N/A	1.5 $\mu\text{m}$

Note: The wear results are reported in the units and precision given in the individual journal publications.

disk is lower than that of a machined or sandblasted titanium pin because it reduced contact between the protruding texture features [89]. Wei et al. laser-treated CoCrMo disks to fabricate a hardened surface with a wavy texture pattern with a period of 8  $\mu\text{m}$  [90]. They performed BoD experiments using a stainless steel ball and the laser-treated CoCrMo disks and showed that the textured disk reduced the friction coefficient by 64% compared to an untreated, smooth CoCrMo disk, which they attributed to reduced contact from the texture features, increased hardness from the laser treatment, and wear debris accumulated in the texture features to reduce third-body abrasive contact. Kustandi et al. performed BoD experiments using a silicon nitride ball articulating with a grooved UHMWPE surface consisting of 1  $\mu\text{m}$  deep by 1  $\mu\text{m}$  wide grooves oriented perpendicular to the sliding direction and measured that the friction coefficient decreased by 35% when articulating with the grooved compared to a smooth UHMWPE disk because the groove texture features reduced the nominal contact area [91]. Choudhury et al. performed PoD experiments using a UHMWPE pin articulating with a textured ceramic disk and documented that the friction coefficient and wear increase for the textured compared to the smooth disk because the soft UHMWPE deformed into the texture features, increasing the contact area, and causing abrasive wear between the UHMWPE and the edges of the texture features [92].

Numerical simulations have also been performed to understand the effect of contact area reduction of textured bearing surfaces on friction and wear. Pakhaliuk et al. used finite element analysis (FEA) to show that spherical texture features on the bearing surface of CoCrMo femoral heads locally increase the contact pressure at the edge of the texture features but reduce the contact pressure at all other points on the UHMWPE and CoCrMo acetabular liners compared to smooth femoral heads because the acetabular liner does not experience compressive stress in the area with texture features on the femoral head [93]. They also showed that rounded edges or fillets locally reduce the contact pressure at the edge of the texture features compared to texture features with “sharp” edges and determined ranges of texture design parameters ( $0.08 \leq \epsilon \leq 0.25$ ,  $0.02 \leq S_p \leq 0.46$ ) that maintain a contact pressure below the yield stress at the edge of the texture features for both MoM and MoP configurations. Figure 8(a) shows FEA results of the contact pressure on a textured CoCrMo surface (in MPa) with  $\epsilon = 0.28$  and  $S_p = 0.13$  in contact with a UHMWPE surface [93]. We observe that areas of elevated contact pressure occur around the edges of the texture features as a result of stress concentrations. Wang et al. also performed FEA simulations of contact between a

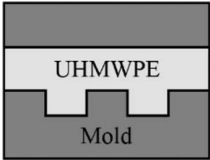
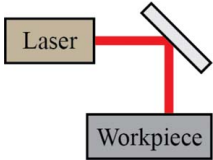
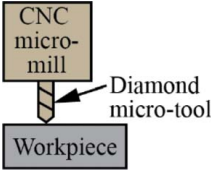
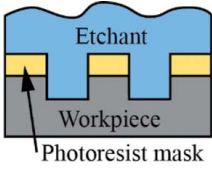
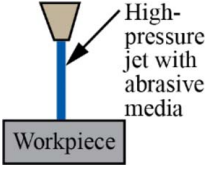
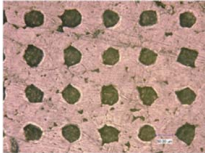
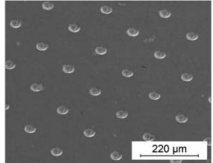
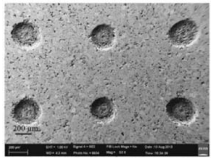
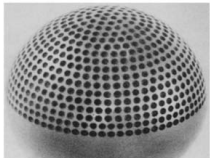
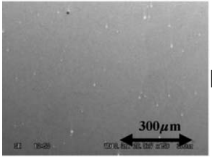
smooth stainless steel surface and UHMWPE and SiC surfaces with cylindrical texture features and showed that elevated contact pressure concentrates around the edges of the texture features on the stiff SiC surface, but smaller stress concentrations exist on the soft UHMWPE surface [94]. Figure 8(b) shows the contact pressure along the centerline and near the edge of a texture feature for the stiff SiC (black line) and soft UHMWPE (red line) [94]. Based on their simulations, Wang et al. concluded that it is advantageous to spread out the regions of elevated local contact pressure by designing texture patterns such that the texture density decreases with increasing stiffness of the textured bearing surface material. They also simulated contact between a textured stainless steel surface and smooth UHMWPE surface to show how the soft bearing surfaces may penetrate the texture features on the hard bearing surface. Figure 8(c) shows the deformation of the smooth UHMWPE surface (in meters) in contact with the textured stainless steel surface [94]. Dong et al. performed simulations of contact between a smooth steel femoral head and a textured UHMWPE acetabular liner to compute the contact pressure, temperature increase, and polyethylene wear [95]. They compared their simulated results to pendulum HJS experiments of a steel femoral head and textured UHMWPE acetabular liner and found that surface texture led to fluctuating local temperature and contact pressure, which led to discontinuous regions of wear on the UHMWPE acetabular liner.

Table 3 summarizes each paper included in this review which used texture features to reduce the nominal contact area between the bearing surfaces. Note that most values in the table are reported with standard units and consistent significant digits. However, we have reported the wear measurements in the units and with the precision provided by each individual publication.

**2.5 Intellectual Property.** In addition to journal publications, several patents have been issued related to different aspects of textured orthopedic biomaterials with application in prosthetic hip or knee implants. We categorize these patents similarly to the journal publications we discussed, i.e., by texture function.

Most of these patents describe embodiments in which textured surfaces serve as lubricant reservoirs and/or accumulate wear debris. For instance, Lilley proposed a prosthetic hip implant made of ceramic materials where the femoral head and acetabular liner each had at least one small reservoir designed to accumulate wear debris [96]. Frey described an acetabular liner with a groove to distribute lubricant to the bearing interface [97]. Legrand also designed a circumferential groove, or “throat,” in an acetabular

**Table 4 Summary and comparison of manufacturing processes to fabricate texture features on orthopedic biomaterials**

Process	Molding	Optical techniques	Conventional machining	Electrochemical processes	Solid particle erosion
Schematic					
Picture	 [54]	 [40]	 [71]	 [38]	 [47]
References	[53,54,91]	[40,48,52,56,59,61,63–67,69,72,73,90]	[39,41,44–46,49–51,58,62,68,70,71,74,92]	[38,42–44,54,55,89]	[47]
Applicable biomaterials	UHMWPE	UHMWPE, CoCrMo, stainless steel, ceramic	UHMWPE, CoCrMo, stainless steel, titanium, ceramic	CoCrMo, stainless steel, titanium	CoCrMo
Range of texture dimensions	1–200 $\mu\text{m}$ diameter, 1–15 $\mu\text{m}$ depth	10–250 $\mu\text{m}$ diameter, 0.5–120 $\mu\text{m}$ depth	55–1000 $\mu\text{m}$ diameter, 1.5–1000 $\mu\text{m}$ depth	50–1000 $\mu\text{m}$ diameter, 3–100 $\mu\text{m}$ depth	0.25–4.40 $\mu\text{m}$ depth
Dimensional accuracy	Good [91]	Good [73]	Fair [41]	Fair [54]	Poor [47]
Throughput	Slow [53]	Fast [40]	Medium–fast [41]	Slow [42]	Medium [47]
Curved surfaces	No [54]	Yes [61]	Yes [39]	Yes [38]	No [47]
Scalable to macroscale areas	Fair [53]	Good [61]	Good [58]	Good [38]	Fair [47]

liner to collect lubricant [98]. Mathys designed an acetabular liner with a single chamber positioned at the point of maximum loading to promote hydrostatic support and lubrication of the femoral head [99]. Yuhta et al. documented bearing surfaces with recessed patterns to retain lubricant in the bearing region and resist wear and adhesion [100]. Burkinshaw described bearing surfaces with evenly distributed “plateaus” and “valleys” to facilitate lubrication [101]. Grundei and Thomas patented bearing surfaces with regularly spaced recesses to act as lubricant reservoirs [102]. Schmid described engineered surfaces for prosthetic hip or knee implants with texture features designed to entrain lubricant in the loaded region and prevent lubricant escape [103].

Only one patent describes the texture function of microhydrodynamic bearings on the surface of prosthetic hip implants. Raeymaekers and Sanders proposed the idea of concave features designed to compress lubricant and facilitate hydrodynamic lubrication to reduce wear [104].

A few patents describe the idea of modifying the contact area to reduce the friction coefficient and/or wear of a prosthetic hip implant. Serbousek and Bono designed an “interrupted” articular face with grooves or texture features on the surface to reduce the articulating surface area of a prosthetic hip or knee implant [105]. Salehi et al. proposed reducing the bearing area with indentations on the surface to reduce the wear [106]. Chan and Ochoa described applying surface textures to reach an optimum contact area in order to reduce wear and increase the lubricity of a prosthetic hip or knee implant [107].

### 3 Manufacturing Textured Bearing Surfaces for Prosthetic Hip Implants

Several processes exist to manufacture texture features on the surfaces of orthopedic biomaterials, including molding, optical techniques, conventional machining, electrochemical processes, and solid particle erosion methods.

While metal components of prosthetic hip implants are commonly cast and then machined [108], molding texture features apply only to a soft UHMWPE surface. The UHMWPE is heated near the glass transition temperature and pressed into a textured mold, which typically comprises hard silicon or copper surfaces with texture features fabricated using e.g., photolithography micro-machining, to reform the UHMWPE to the negative shape of the mold [53,91]. Advanced molding techniques, such as nanoimprint lithography, have produced texture features smaller than  $1\ \mu\text{m}$  in UHMWPE [91], and smaller than 10 nm in polymers such as PMMA [109]. However, molding is time-intensive and requires special mold designs and process optimization to fabricate texture features on e.g., curved surfaces [110], which is important in the context of prosthetic hip implants.

Optical, i.e., laser-based techniques offer flexibility for texturing orthopedic biomaterials because these techniques are fast and can cover curved surfaces. Ultra-short pulsed lasers focus on a small area of the workpiece and locally ablate the material, leaving a small indentation [111]. Controlling the laser parameters such as power, pulse duration, and optical focus customizes the process for different materials and texture designs [112]. Because lasers are electromagnetic waves, they also enable other techniques, such as diffraction laser ablation, where the laser beam shines through a small aperture, resulting in diffraction patterns that ablate material in concentric ring patterns [56]. Further, laser interference lithography focuses multiple laser beams on the surface such that areas of additive interference are ablated, whereas areas of subtractive interference remain unaffected by the laser, resulting in a surface with a wave-like texture pattern [90]. Laser-based methods are fast, precise, and have minimal impact on the surrounding material surface (depending on the laser parameters) [113]. However, laser ablation can leave behind a material build-up around the edges of the texture features because of the re-deposition of ablated material [114]. This occurs primarily with long pulse-

length lasers, i.e., nano- and pico-second as opposed to femto-second lasers [115]. Additionally, the high heat may locally affect the material microstructure and hardness [114].

Conventional machining has also been used to texture orthopedic biomaterials. Indentation operates by pressing a hard (often diamond-tipped) indenter into the workpiece [74]. The indenter can have different shapes, and the combination of the indentation load and material hardness determines the depth of the resulting texture features. However, an indentation may cause residual stresses and the build-up of ridges around the texture features from the displaced material [74,116]. Micro-milling operates similarly to conventional milling, but with smaller tools to accommodate the small dimensions of the texture features. Five-axis computer numerical control (CNC) machines have been used to manufacture texture features on spherical surfaces such as a femoral head or acetabular liner [39]. Diamond or carbide cutting tools are required when machining hard material such as ceramic [71], and the cutting tools must be replaced frequently to maintain accuracy [70]. End-milling is a fast alternative for machining texture features with a small aspect ratio, where a spherical shaped end-mill touches the surface, and leaves a small spherical indentation [41,49].

Electrochemical processes manufacture texture features by selectively etching the material through chemical and/or electrical means. A mask protects areas where no etching may occur when the entire surface is exposed to a reactive chemical [89] or an electrolyte bath and direct current voltage [117]. Thus, only the unmasked areas of the surface are selectively etched until the desired texture features are formed, and the mask can be removed. Masks are typically manufactured using photolithography and are mostly used for flat surfaces [54], but have been applied to spherical surfaces too [38]. The etchant must be selected for a specific material and electrolytic etching is only used for metallic surfaces. Electrical discharge machining (EDM) operates similarly to electrolytic etching, but a specific tool geometry is used as an electrode to create sparks that erode the material (“sinker EDM”) [118]. EDM is typically slower than other manufacturing processes but can produce very precise texture features, depending on the tool geometry.

Solid particle erosion methods spray small particles of abrasive media in a high-pressure jet of air or water to cut through or roughen the surface of a workpiece. The size, shape, and concentration of texture features after solid particle erosion display a degree of randomness but depend on the properties of the abrasive particles, and the nozzle size and jet pressure [119]. We note that solid particle erosion does not allow for precise control of the texture feature geometry, density, or location, and it may be used in conjunction with other texturing techniques to produce multi-scale roughened texture features [120].

Table 4 shows a comparison of the different categories of manufacturing processes of texture features that have been used in the context of texturing orthopedic biomaterials. For each manufacturing process, we include a schematic of the working principle, a picture of fabricated texture features, references to publications where the process has been documented, the type of orthopedic biomaterials that have been textured, the range of texture feature geometries, and several qualitative metrics to compare the different processes with each other. Each qualitative metric is described as follows, and each designation in Table 4 is referenced as justification. The dimensional accuracy metric is based on the range of texture feature geometries produced by each process, where good dimensional accuracy means the process can produce texture features with a diameter smaller than  $25\ \mu\text{m}$ , and poor dimensional accuracy means the process cannot control the texture feature diameter. The throughput metric describes the processing time for each process, based on descriptions in the references. The curved surface metric describes whether each process has been used to fabricate texture features on a curved surface (such as a femoral head and/or acetabular shell/liner), and the scalable to macroscale areas metric is based on the surface area that has been textured with each process, where we distinguish between good and fair

scalability at approximately 1200 mm<sup>2</sup>, which is equivalent to the surface area of a 28 mm diameter acetabular liner.

#### 4 Discussion

Texture features may serve three different functions to reduce the friction coefficient and wear of the bearing surfaces and, thus, must be designed with a specific application in mind. Prosthetic hip implants represent a complex engineering application, and manufacturing texture features on the bearing surfaces of prosthetic hip implants show promise for a personalized medicine approach that customizes prosthetic hip implant bearing surfaces for specific patient lifestyles. “Personalized medicine” typically refers to tailored pharmaceuticals to match a specific patient’s genetics [121], but can also apply to customize medical devices to mitigate risks and improve the success of surgery outcomes by accounting for the specifics of each individual patient [122]. In the past, customizing prosthetic hip implants has been limited to different bearing material choices and modular designs that allow sizing the different components of a prosthetic hip implant to best reconstruct the patient’s anatomy [123].

However, this review shows that texture design parameters, in combination with different bearing operating conditions, affect the lubrication of the bearing surfaces of a prosthetic hip implant (or orthopedic biomaterials used in the context of prosthetic hip implants). For example, Zhang et al. showed for textured UHMWPE articulating with stainless steel, the optimum texture aspect ratio to minimize the friction coefficient and wear increases with increasing bearing load-carrying capacity [53]. Similarly, Allen and Raeymaekers showed for textured CoCrMo articulating with UHMWPE that the optimum texture aspect ratio to maximize the lubricant film thickness increases with increasing flow parameter and decreasing bearing load-carrying capacity [83]. Additionally, changing the bearing surface material combination or changing which bearing surface material is textured drastically affects the optimum texture design parameters, as shown by Zhang et al. [54] and Wang et al. [94]. Thus, by changing the texture design parameters, a prosthetic hip implant could be tailored to perform optimally for specific patients’ anatomy, body mass, and lifestyle activity level. Surgeons could create a personalized medicine decision matrix that considers the texture design parameters in addition to the size and materials of a prosthetic hip implant to best suit each individual patient. Figure 9 shows a schematic of potential input parameters (age, body mass, activity level) and output parameters (bearing material pair, texture aspect ratio, texture density) that one may consider in a textured prosthetic hip implant personalized medicine decision matrix.

Several challenges must be overcome before textured prosthetic hip implants can be designed and manufactured for in-vivo use,

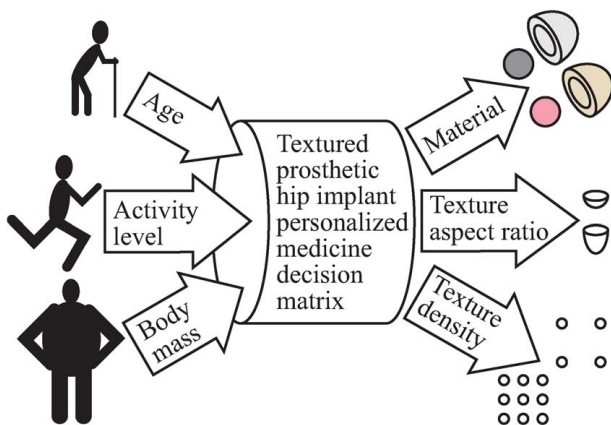


Fig. 9 Input and output parameters for personalized textured prosthetic hip implants

including dynamic hip joint simulator experiments, manufacturing concerns, and regulatory approval. To be approved by the US Food and Drug Administration (FDA), a new medical device design must be substantially equivalent to an approved predicate device or undergo thorough and expensive testing to obtain a new pre-market approval (“De Novo” classification). To show substantial equivalence to an approved predicate device, the new device must have the same intended use as the predicate device, it must not raise any new concerns about safety or effectiveness, and it must demonstrate equivalent safety and effectiveness as the predicate device [124]. While textured prosthetic hip implants have the same intended use as traditional prosthetic hip implants, they will likely raise new concerns about safety and effectiveness.

Langhorne et al. tested the corrosion potential of laser-textured CoCrMo surfaces and found no significant difference to untreated CoCrMo surfaces, indicating that texture features will not likely increase the corrosion of biomedical CoCrMo alloys [66]. However, residual stresses from micromachining the texture features may locally affect the hardness and fracture toughness of the material. Roy et al. measured compressive residual stresses and a reduced fracture toughness inside the texture features on ceramic surfaces, in addition to tensile residual stresses and a reduced hardness close to the edges of the texture features [70]. The change of fracture toughness inside the texture features might not affect the performance of the prosthetic hip implant, as this portion of the surface will not contact another solid surface. However, the tensile residual stresses around the texture contour could cause an increased risk of fracture. Choudhury et al. showed reduced hardness around the contour of the texture features on a stainless steel surface and proposed using hard surface coatings to counteract the problem [42]. Further, Lee et al. showed that a hardened thermal oxidation layer protected the texture features on the surface of titanium, while untreated texture features were deformed and worn away [50].

Also, heat from laser texturing processes may affect the microstructure and hardness of the bearing materials. However, laser operating parameters may be altered to reduce thermal effects, while avoiding material re-deposition around the contour of the texture features. In contrast, Wei et al. documented improved material properties after laser-treatments reduced the grain size and increased the hardness of CoCrMo surfaces [90].

A major concern for the longevity of prosthetic hip implants is wear debris that can affect the tissue surrounding the prosthetic implant. The vast majority of the literature shows that texture features on the bearing surfaces of orthopedic biomaterials reduce wear debris [38,46,47,65,71]. However, a few data points indicate increased wear for specific texture features and operating conditions [45,55]. Thus, it is important to design texture features for the specific bearing operating conditions to reduce wear and improve prosthetic hip implant longevity.

Other key challenges to overcome are specific to the hard-on-soft configurations. Texture features on the hard surface perform well at low bearing loads but may experience increased friction coefficient and wear at high bearing load-carrying capacity, presumably because the soft material of the counterface can deform and penetrate into the texture features [54,63,92]. One solution to this problem is applying the texture features on the soft surface. While the texture features on the soft surface require a different set of optimum texture design parameters, the literature shows that they reduce the friction coefficient and wear even at high bearing load-carrying capacity [54]. However, as the soft surface wears faster than the hard surface, the texture features may eventually wear away, or have their optimum geometry changed by wear. Based upon wear-rates published in Ref. [65], it would take approximately 732,000 cycles (less than 1 year for the average adult) to completely remove 1 μm deep texture features from the surface of a UHMWPE acetabular liner. For a more wear-resistant VEXPE acetabular liner, it would take approximately 3,173,000 cycles (just over 3 years) to wear away these same shallow texture features and lose the benefit of a textured bearing surface.

Another difficulty is a lack of experimentally validated boundary/mixed lubrication regime numerical models for textured orthopedic biomaterials. The majority of the numerical simulations of textured orthopedic biomaterials require the assumption of full-film lubrication, i.e., no solid-on-solid contact. This simplification enables using the Reynolds equation to solve for the lubricant film pressure and thickness, but full-film lubrication is only realistic for a portion of the gait cycle. For approximately half of a typical gait cycle, a prosthetic hip implant operates in the boundary/mixed lubrication regime [125]. Thus, it is important to model realistic surface contact to accurately capture the lubrication of textured prosthetic hip implant bearings throughout the entire gait cycle. Only Gao et al. [86–88] and Basri et al. [85] have incorporated both lubricant film pressure and solid-on-solid contact into the same model of textured orthopedic biomaterials. In the future, mixed lubrication numerical models will greatly assist the design of optimum texture design parameters covering the entire gait cycle and will need experimental validation to ensure accuracy.

No friction or wear experiments of textured prosthetic hip implants have been performed with hip joint simulators using traditional dynamic loading and kinematic cycles that mimic in-vivo gait (e.g., Paul's curve [126]). The guidelines in the ISO 14242 standard impose a range of sliding parameters approximately between  $7.8 \cdot 10^{-12}$  and  $3.3 \cdot 10^{-10}$ , similar to the most common ranges used in the literature for pendulum HJS, PoD, RoD, hybrid, and BoD experiments with simplified geometry, kinematics, and loading (see Fig. 5). While these studies have evaluated operating conditions within a realistic range, it will be important to evaluate dynamically changing conditions as occurs in an in-vivo prosthetic hip implant. Experiments with realistic geometries, kinematics, and loading will be necessary to prove the safety and effectiveness of textured prosthetic hip implants before consideration for clinical trials and/or FDA approval.

## 5 Conclusions

We conclude the following:

- (1) Texture features on the bearing surfaces of orthopedic biomaterials perform three potential functions to reduce friction and wear: (1) lubricant reservoirs and accumulating wear debris, (2) micro-hydrodynamic bearings, and (3) reducing the nominal contact area. Reviewing the literature relevant to prosthetic hip implants reveals trends to guide the design of textured bearing surfaces for these different texture functions. Specifically, texture features that function as lubricant reservoirs have aspect ratios greater than 0.1 whereas texture features that function as micro-hydrodynamic bearings have aspect ratios smaller than 0.1. Texture features that only reduce the contact area operate in the boundary lubrication regime, and their effectiveness is independent of the texture aspect ratio and entirely driven by the texture density.
- (2) The literature shows that depending on the specific texture design parameters, textured bearings perform differently with different materials and different operating conditions. Thus, this shows promise to tailor textured bearing surfaces of prosthetic hip implants to account for patient-specific factors including age, weight, and lifestyle (activity level).
- (3) Many techniques exist to manufacture texture features on the surface of orthopedic biomaterials. Optical (laser-based) techniques display the greatest flexibility, speed, and precision for textured prosthetic hip implants.

## Acknowledgment

This work was supported by the National Institutes of Health, National Institute of Arthritis and Musculoskeletal and Skin Diseases under Grant 1R03AR066826-01A1.

## Conflict of Interest

There are no conflicts of interest.

## Data Availability Statement

The datasets generated and supporting the findings of this article are obtainable from the corresponding author upon reasonable request. The authors attest that all data for this study are included in the paper. Data provided by a third party are listed in Acknowledgment.

## References

- [1] Sloan, M., Premkumar, A., and Sheth, N. P., 2018, "Projected Volume of Primary Total Joint Arthroplasty in the U.S., 2014 to 2030," *J. Bone Jt. Surg. – Am.*, **100**(17), pp. 1455–1460.
- [2] Ravi, B., Croxford, R., Reichmann, W. M., Losina, E., Katz, J. N., and Hawker, G. A., 2012, "The Changing Demographics of Total Joint Arthroplasty Recipients in the United States and Ontario From 2001 to 2007," *Best Pract. Res. Clin. Rheumatol.*, **26**(5), pp. 637–647.
- [3] Borjali, A., 2018, *A Patterned Microtexture to Reduce Polyethylene Wear in Metal-on-Polyethylene Bearings, With Application in Prosthetic Hip Implants*, University of Utah, Salt Lake City, UT.
- [4] Foran, J. R. H., 2015, "Total Hip Replacement," *Am. Acad. Orthop. Surg.*, <https://orthoinfo.aaos.org/en/treatment/total-hip-replacement>, Accessed 21 May 2019.
- [5] Epinette, J.-A., and Manley, M. T., 2014, "No Differences Found in Bearing Related Hip Survivorship at 10–12 Years Follow-up Between Patients With Ceramic on Highly Cross-Linked Polyethylene Bearings Compared to Patients With Ceramic on Ceramic Bearings," *J. Arthroplasty*, **29**(7), pp. 1369–1372.
- [6] Rieker, C., Konrad, R., and Schoun, R., 2001, "In Vitro Comparison of the Two Hard-Hard Articulations for Total Hip Replacements," *Proc. Inst. Mech. Eng. Part H - J. Eng. Med.*, **215**(2), pp. 153–160.
- [7] Bosker, B. H., Ettema, H. B., Boomsma, M. F., Kollen, B. J., Maas, M., and Verheyen, C. C. P. M., 2012, "High Incidence of Pseudotumour Formation After Large-Diameter Metal-on-Metal Total Hip Replacement," *J. Bone Joint Surg. Br.*, **94-B**(6), pp. 755–761.
- [8] Milošev, I., Kovač, S., Trebše, R., Levašič, V., and Pišot, V., 2012, "Comparison of Ten-Year Survivorship of Hip Prostheses With Use of Conventional Polyethylene, Metal-on-Metal, or Ceramic-on-Ceramic Bearings," *J. Bone Joint Surg.—Ser. A*, **94**(19), pp. 1756–1763.
- [9] Choi, I. Y., Kim, Y. S., Hwang, K. T., and Kim, Y. H., 2010, "Incidence and Factors Associated With Squeaking in Alumina-on-Alumina THA," *Clin. Orthop. Relat. Res.*, **468**(12), pp. 3234–3239.
- [10] Heckmann, N. D., Sivasundaram, L., Steff, M. D., Kang, H. P., Basler, E. T., and Lieberman, J. R., 2018, "Total Hip Arthroplasty Bearing Surface Trends in the United States From 2007 to 2014: The Rise of Ceramic on Polyethylene," *J. Arthroplasty*, **33**(6), pp. 1757–1763.
- [11] Evans, J. T., Evans, J. P., Walker, R. W., Blom, A. W., Whitehouse, M. R., and Sayers, A., 2019, "How Long Does a Hip Replacement Last? A Systematic Review and Meta-Analysis of Case Series and National Registry Reports With More Than 15 Years of Follow-Up," *Lancet*, **393**(10172), pp. 647–654.
- [12] Rajaei, S. S., Campbell, J. C., Mirocha, J., and Paiement, G. D., 2018, "Increasing Burden of Total Hip Arthroplasty Revisions in Patients Between 45 and 64 Years of Age," *J. Bone Joint Surg.*, **100**(6), pp. 449–458.
- [13] Bozic, K. J., Kamath, A. F., Ong, K., Lau, E., Kurtz, S., Chan, V., Vail, T. P., Rubash, H., and Berry, D. J., 2015, "Comparative Epidemiology of Revision Arthroplasty: Failed THA Poses Greater Clinical and Economic Burdens Than Failed TKA," *Clin. Orthop. Relat. Res.*, **473**(6), pp. 2131–2138.
- [14] Liu, A., Richards, L., Bladen, C. L., Ingham, E., Fisher, J., and Tipper, J. L., 2015, "The Biological Response to Nanometre-Sized Polymer Particles," *Acta Biomater.*, **23**, pp. 38–51.
- [15] Harris, W. H., 2001, "Wear and Periprosthetic Osteolysis: The Problem," *Clin. Orthop. Relat. Res.*, **393**, pp. 66–70.
- [16] Woolf, S. H., and Schoomaker, H., 2019, "Life Expectancy and Mortality Rates in the United States, 1959–2017," *JAMA—J. Am. Med. Assoc.*, **322**(20), pp. 1996–2016.
- [17] Laurent, M. P., Johnson, T. S., Crowninshield, R. D., Blanchard, C. R., Bhambri, S. K., and Yao, J. Q., 2008, "Characterization of a Highly Cross-Linked Ultrahigh Molecular-Weight Polyethylene in Clinical Use in Total Hip Arthroplasty," *J. Arthroplasty*, **23**(5), pp. 751–761.
- [18] Kurtz, S. M., 2004, *The UHMWPE Handbook: Ultra-High Molecular Weight Polyethylene in Total Joint Replacement*, Academic Press, Amsterdam.
- [19] Lerf, R., Zurbrugg, D., and Delfosse, D., 2010, "Use of Vitamin E to Protect Cross-Linked UHMWPE From Oxidation," *Biomaterials*, **31**(13), pp. 3643–3648.
- [20] Haider, H., Weisenburger, J. N., Kurtz, S. M., Rimnac, C. M., Freedman, J., Schroeder, D. W., and Garvin, K. L., 2012, "Does Vitamin E-Stabilized Ultrahigh-Molecular-Weight Polyethylene Address Concerns of Cross-Linked Polyethylene in Total Knee Arthroplasty?," *J. Arthroplasty*, **27**(3), pp. 461–469.

- [21] Rowell, S. L., and Muratoglu, O. K., 2016, "Investigation of Surgically Retrieved, Vitamin E-Stabilized, Crosslinked UHMWPE Implants After Short-Term in Vivo Service," *J. Biomed. Mater. Res.—Part B Appl. Biomater.*, **104B**(6), pp. 1132–1140.
- [22] Brizuela, M., Garcia-Luis, A., Viviente, J. L., Braceras, I., and Oñate, J. I., 2002, "Tribological Study of Lubricious DLC Biocompatible Coatings," *J. Mater. Sci. Mater. Med.*, **13**(12), pp. 1129–1133.
- [23] Balagna, C., Faga, M. G., and Spriano, S., 2012, "Tantalum-Based Multilayer Coating on Cobalt Alloys in Total Hip and Knee Replacement," *Mater. Sci. Eng. C*, **32**(4), pp. 887–895.
- [24] Ching, H. A., Choudhury, D., Nine, M. J., and Abu Osman, N. A., 2014, "Effects of Surface Coating on Reducing Friction and Wear of Orthopaedic Implants," *Sci. Technol. Adv. Mater.*, **15**(1), p. 014402.
- [25] Rahaman, M. N., Yao, A., Bal, B. S., Garino, J. P., and Ries, M. D., 2007, "Ceramics for Prosthetic Hip and Knee Joint Replacement," *J. Am. Ceram. Soc.*, **90**(7), pp. 1965–1988.
- [26] Ibatan, T., Uddin, M. S., and Chowdhury, M. A. K., 2015, "Recent Development on Surface Texturing in Enhancing Tribological Performance of Bearing Sliders," *Surf. Coatings Technol.*, **272**, pp. 102–120.
- [27] Gropper, D., Wang, L., and Harvey, T. J., 2016, "Hydrodynamic Lubrication of Textured Surfaces: A Review of Modeling Techniques and Key Findings," *Tribol. Int.*, **94**, pp. 509–529.
- [28] Zhang, H., Hua, M., Dong, G. N., Zhang, D. Y., and Chin, K. S., 2016, "A Mixed Lubrication Model for Studying Tribological Behaviors of Surface Texturing," *Tribol. Int.*, **93**(Part B), pp. 583–592.
- [29] Ryk, G., Kligerman, Y., and Etsion, I., 2002, "Experimental Investigation of Laser Surface Texturing for Reciprocating Automotive Components," *Tribol. Trans.*, **45**(4), pp. 444–449.
- [30] Varenberg, M., Halperin, G., and Etsion, I., 2002, "Different Aspects of the Role of Wear Debris in Fretting Wear," *Wear*, **252**(11–12), pp. 902–910.
- [31] Brizmer, V., Kligerman, Y., and Etsion, I., 2003, "A Laser Surface Textured Parallel Thrust Bearing," *Tribol. Trans.*, **46**(3), pp. 397–403.
- [32] Dobrica, M. B., Fillon, M., Pascovici, M. D., and Cicone, T., 2010, "Optimizing Surface Texture for Hydrodynamic Lubricated Contacts Using a Mass-Conserving Numerical Approach," *Proc. Inst. Mech. Eng. Part J-J. Eng. Tribol.*, **224**(8), pp. 737–750.
- [33] Noutary, M.-P., Biboulet, N., and Lubrecht, A. A., 2020, "Dimple Influence on Load Carrying Capacity of Parallel Surfaces," *Tribol. Int.*, **149**, p. 105452.
- [34] Lu, A., Gao, Y., Jin, T., Luo, X., Zeng, Q., and Shang, Z., 2020, "Effects of Surface Roughness and Texture on the Bacterial Adhesion on the Bearing Surface of Bio-Ceramic Joint Implants: An in Vitro Study," *Ceram. Int.*, **46**(5), pp. 6550–6559.
- [35] Qin, L., Zeng, Q., Wang, W., Zhang, Y., and Dong, G., 2014, "Response of MC3T3-E1 Osteoblast Cells to the Microenvironment Produced on Co-Cr-Mo Alloy Using Laser Surface Texturing," *J. Mater. Sci.*, **49**(6), pp. 2662–2671.
- [36] Myant, C., Underwood, R., Fan, J., and Cann, P. M., 2012, "Lubrication of Metal-on-Metal Hip Joints: The Effect of Protein Content and Load on Film Formation and Wear," *J. Mech. Behav. Biomed. Mater.*, **6**, pp. 30–40.
- [37] Etsion, I., 2013, "Modeling of Surface Texturing in Hydrodynamic Lubrication," *Friction*, **1**(3), pp. 195–209.
- [38] Ito, H., Kaneda, K., Yuhta, T., Nishimura, I., Yasuda, K., and Matsuno, T., 2000, "Reduction of Polyethylene Wear by Concave Dimples on the Frictional Surface in Artificial Hip Joints," *J. Arthroplasty*, **15**(3), pp. 332–338.
- [39] Sagbas, B., and Durakbasa, M. N., 2013, "Effect of Surface Patterning on Frictional Heating of Vitamin E Blended UHMWPE," *Wear*, **303**(1–2), pp. 313–320.
- [40] Tarabolsi, M., Klassen, T., Mantwill, F., Gärtner, F., Siegel, F., and Schulz, A.-P., 2013, "Patterned CoCrMo and Al<sub>2</sub>O<sub>3</sub> Surfaces for Reduced Free Wear Debris in Artificial Joint Arthroplasty," *J. Biomed. Mater. Res.—Part A*, **101A**(12), pp. 3447–3456.
- [41] Nečas, D., Usami, H., Niimi, T., Sawae, Y., Krupka, I., and Hartl, M., 2020, "Running-in Friction of Hip Joint Replacements Can Be Significantly Reduced: The Effect of Surface-Textured Acetabular Cup," *Friction*, **8**(6), pp. 1137–1152.
- [42] Choudhury, D., Ay Ching, H., Mamat, A. B., Cizek, J., Abu Osman, N. A., Vrbka, M., Hartl, M., and Krupka, I., 2015, "Fabrication and Characterization of DLC Coated Microdimples on Hip Prosthesis Heads," *J. Biomed. Mater. Res.—Part B Appl. Biomater.*, **103**(5), pp. 1002–1012.
- [43] Choudhury, D., Urban, F., Vrbka, M., Hartl, M., and Krupka, I., 2015, "A Novel Tribological Study on DLC-Coated Micro-Dimpled Orthopedics Implant Interface," *J. Mech. Behav. Biomed. Mater.*, **45**, pp. 121–131.
- [44] Nishimura, I., Yuhta, T., Ikubo, K., Shimooka, T., Murabayashi, S., and Mitamura, Y., 1993, "Modification of the Frictional Surfaces of Artificial Joints," *ASAIO J.*, **39**(3), pp. M762–M766.
- [45] Young, S. K., Lotito, M. A., and Keller, T. S., 1998, "Friction Reduction in Total Joint Arthroplasty," *Wear*, **222**(1), pp. 29–37.
- [46] Sagbas, B., and Durakbasa, M. N., 2014, "Surface Texturing of Vitamin E Blended UHMWPE for Reduction of Wear," *Acta Phys. Pol. A*, **125**(2), pp. 481–483.
- [47] Sawano, H., Warisawa, S., and Ishihara, S., 2009, "Study on Long Life of Artificial Joints by Investigating Optimal Sliding Surface Geometry for Improvement in Wear Resistance," *Precis. Eng.*, **33**(4), pp. 492–498.
- [48] Guo, J., Mei, T., Li, Y., Ren, S., Hafezi, M., Lu, H., and Dong, G., 2018, "Sustained-Release Application of PCEC Hydrogel on Laser-Textured Surface Lubrication," *Mater. Res. Express*, **5**(6), p. 065315.
- [49] Pratap, T., and Patra, K., 2020, "Tribological Performances of Symmetrically Micro-Textured Ti-6Al-4V Alloy for Hip Joint," *Int. J. Mech. Sci.*, **182**, p. 105736.
- [50] Lee, H., Lee, S., Park, J.-K., and Yang, M., 2018, "Friction and Wear Characteristics of Surface-Modified Titanium Alloy for Metal-on-Metal Hip Joint Bearing," *Int. J. Precis. Eng. Manuf.*, **19**(6), pp. 917–924.
- [51] López-Cervantes, A., Domínguez-López, I., Barceñas-Sánchez, J. D. O., and García-García, A. L., 2013, "Effects of Surface Texturing on the Performance of Biocompatible UHMWPE as a Bearing Material During in Vitro Lubricated Sliding/Rolling Motion," *J. Mech. Behav. Biomed. Mater.*, **20**, pp. 45–53.
- [52] Sufyan, M., Hussain, M., Ahmad, H., Abbas, N., Ashraf, J., and Zahra, N., 2019, "Bulge Micro-Textures Influence on Tribological Performance of Ultra-High-Molecular-Weight-Polyethylene (UHMWPE) Under Phosphatidylcholine (Lipid) and Bovine Serum Albumin (BSA) Solutions," *Biomed. Phys. Eng. Express*, **5**(3), p. 035021.
- [53] Zhang, B., Huang, W., and Wang, X., 2012, "Biomimetic Surface Design for Ultrahigh Molecular Weight Polyethylene to Improve the Tribological Properties," *Proc. Inst. Mech. Eng. Part J J. Eng. Tribol.*, **226**(8), pp. 705–713.
- [54] Zhang, B., Huang, W., Wang, J., and Wang, X., 2013, "Comparison of the Effects of Surface Texture on the Surfaces of Steel and UHMWPE," *Tribol. Int.*, **65**, pp. 138–145.
- [55] Wang, M., Zhang, C., and Wang, X., 2017, "The Wear Behavior of Textured Steel Sliding Against Polymers," *Materials (Basel)*, **10**(4), p. 330.
- [56] Zhang, H., Qin, L., Hua, M., Dong, G., and Chin, K., 2015, "A Tribological Study of the Petaloid Surface Texturing for Co-Cr-Mo Alloy Artificial Joints," *Appl. Surf. Sci.*, **332**, pp. 557–564.
- [57] Sahlin, F., Glavatskih, S. B., Almqvist, T., and Larsson, R., 2005, "Two-Dimensional CFD-Analysis of Micro-Patterned Surfaces in Hydrodynamic Lubrication," *ASME J. Tribol.*, **127**(1), pp. 96–102.
- [58] Dong, Y., Svoboda, P., Vrbka, M., Kostal, D., Urban, F., Cizek, J., Roupčova, P., Dong, H., Krupka, I., and Hartl, M., 2016, "Towards Near-Permanent CoCrMo Prosthesis Surface by Combining Micro-Texturing and Low Temperature Plasma Carburising," *J. Mech. Behav. Biomed. Mater.*, **55**, pp. 215–227.
- [59] Cho, M., and Choi, H.-J., 2014, "Optimization of Surface Texturing for Contact Between Steel and Ultrahigh Molecular Weight Polyethylene Under Boundary Lubrication," *Tribol. Lett.*, **56**(3), pp. 409–422.
- [60] Krupka, I., and Hartl, M., 2007, "The Effect of Surface Texturing on Thin EHD Lubrication Films," *Tribol. Int.*, **40**(7), pp. 1100–1110.
- [61] Choudhury, D., Rebenda, D., Sasaki, S., Hekrlé, P., Vrbka, M., and Zou, M., 2018, "Enhanced Lubricant Film Formation Through Micro-Dimpled Hard-on-Hard Artificial Hip Joint: An in-Situ Observation of Dimple Shape Effects," *J. Mech. Behav. Biomed. Mater.*, **81**, pp. 120–129.
- [62] Choudhury, D., Vrbka, M., Mamat, A. B., Stavness, I., Roy, C. K., Mootanah, R., and Krupka, I., 2017, "The Impact of Surface and Geometry on Coefficient of Friction of Artificial Hip Joints," *J. Mech. Behav. Biomed. Mater.*, **72**, pp. 192–199.
- [63] Chyr, A., Qiu, M., Speltz, J. W., Jacobsen, R. L., Sanders, A. P., and Raeymaekers, B., 2014, "A Patterned Microtexture to Reduce Friction and Increase Longevity of Prosthetic Hip Joints," *Wear*, **315**(1–2), pp. 51–57.
- [64] Qiu, M., Chyr, A., Sanders, A. P., and Raeymaekers, B., 2014, "Designing Prosthetic Knee Joints With Bio-Inspired Bearing Surfaces," *Tribol. Int.*, **77**, pp. 106–110.
- [65] Borjali, A., Langhorn, J., Monson, K., and Raeymaekers, B., 2017, "Using a Patterned Microtexture to Reduce Polyethylene Wear in Metal-on-Polyethylene Prosthetic Bearing Couples," *Wear*, **392–393**, pp. 77–83.
- [66] Langhorn, J., Borjali, A., Hippensteel, E., Nelson, W., and Raeymaekers, B., 2018, "Microtextured CoCrMo Alloy for Use in Metal-on-Polyethylene Prosthetic Joint Bearings: Multi-Directional Wear and Corrosion Measurements," *Tribol. Int.*, **124**, pp. 178–183.
- [67] Borjali, A., Monson, K., and Raeymaekers, B., 2018, "Friction Between a Polyethylene Pin and a Microtextured CoCrMo Disc, and Its Correlation to Polyethylene Wear, as a Function of Sliding Velocity and Contact Pressure, in the Context of Metal-on-Polyethylene Prosthetic Hip Implants," *Tribol. Int.*, **127**, pp. 568–574.
- [68] Dougherty, P. S. M., Srivastava, G., Onler, R., Ozdoganlar, O. B., and Higgs, C. F., 2015, "Lubrication Enhancement for UHMWPE Sliding Contacts Through Surface Texturing," *Tribol. Trans.*, **58**(1), pp. 79–86.
- [69] Kashyap, V., and Ramkumar, P., 2019, "Feasibility Study of Micro-Groove Cross Hatched Surface Texturing on Ti6Al4V for Improved Biotribological Performance in Metal-on-Polymer Hip Implant," *Tribol.—Mater. Surfaces Interfaces*, **13**(3), pp. 150–160.
- [70] Roy, T., Choudhury, D., Bin Mamat, A., and Pingguan-Murphy, B., 2014, "Fabrication and Characterization of Micro-Dimple Array on Al<sub>2</sub>O<sub>3</sub> Surfaces by Using a Micro-Tooling," *Ceram. Int.*, **40**(1 PART B), pp. 2381–2388.
- [71] Roy, T., Choudhury, D., Ghosh, S., Bin Mamat, A., and Pingguan-Murphy, B., 2015, "Improved Friction and Wear Performance of Micro Dimpled Ceramic-on-Ceramic Interface for Hip Joint Arthroplasty," *Ceram. Int.*, **41**(1), pp. 681–690.
- [72] Drescher, P., Oldorf, P., Dreier, T., Peters, R., and Seitz, H., 2019, "Modification of Joint Prosthesis Surfaces by Ultrashort Pulse Laser Treatment for Improved Joint Lubrication," *Curr. Dir. Biomed. Eng.*, **5**(1), pp. 57–60.
- [73] Drescher, P., Oldorf, P., Dreier, T., Schnell, G., Peters, R., and Seitz, H., 2020, "Ring-Shaped Surface Microstructures for Improved Lubrication Performance of Joint Prosthesis," *Lubricants*, **8**(4), p. 45.
- [74] Zhou, X., Galvin, A. L., Jin, Z., Yan, X., and Fisher, J., 2012, "The Influence of Concave Dimples on the Metallic Counterface on the Wear of Ultra-High Molecular Weight Polyethylene," *Proc. Inst. Mech. Eng. Part J J. Eng. Tribol.*, **226**(6), pp. 455–462.

- [75] Han, J., Fang, L., Sun, J., and Ge, S., 2010, "Hydrodynamic Lubrication of Microdimple Textured Surface Using Three-Dimensional CFD," *Tribol. Trans.*, **53**(6), pp. 860–870.
- [76] Gohar, R., and Rahnejat, H., 2008, *Fundamentals of Tribology*, Imperial College Press, Hackensack, NJ.
- [77] Qiu, M., Bailey, B. N., Stoll, R., and Raeymaekers, B., 2014, "The Accuracy of the Compressible Reynolds Equation for Predicting the Local Pressure in Gas-Lubricated Textured Parallel Slider Bearings," *Tribol. Int.*, **72**, pp. 83–89.
- [78] Rahmani, R., and Rahnejat, H., 2018, "Enhanced Performance of Optimised Partially Textured Load Bearing Surfaces," *Tribol. Int.*, **117**, pp. 272–282.
- [79] Qiu, M., and Raeymaekers, B., 2015, "The Load-Carrying Capacity and Friction Coefficient of Incompressible Textured Parallel Slider Bearings With Surface Roughness Inside the Texture Features," *Proc. Inst. Mech. Eng. Part J J. Eng. Tribol.*, **229**(4), pp. 547–556.
- [80] Zhang, Y. L., Zhang, X. G., and Matsoukas, G., 2015, "Numerical Study of Surface Texturing for Improving Tribological Properties of Ultra-High Molecular Weight Polyethylene," *Biosurf. Biotribol.*, **1**(4), pp. 270–277.
- [81] Shen, C., and Khonsari, M. M., 2015, "Numerical Optimization of Texture Shape for Parallel Surfaces Under Unidirectional and Bidirectional Sliding," *Tribol. Int.*, **82**(Part A), pp. 1–11.
- [82] Su, B., Huang, L., Huang, W., and Wang, X., 2017, "The Load Carrying Capacity of Textured Sliding Bearings With Elastic Deformation," *Tribol. Int.*, **109**, pp. 86–96.
- [83] Allen, Q., and Raeymaekers, B., 2020, "Maximizing the Lubricant Film Thickness Between a Rigid Microtextured and a Smooth Deformable Surface in Relative Motion, Using a Soft Elasto-Hydrodynamic Lubrication Model," *ASME J. Tribol.*, **142**(7), p. 071802.
- [84] Allen, Q., and Raeymaekers, B., 2021, "The Effect of Texture Floor Profile on the Lubricant Film Thickness in a Textured Hard-on-Soft Bearing With Relevance to Prosthetic Hip Implants," *ASME J. Tribol.*, **143**(2), p. 021801.
- [85] Basri, H., Syahrom, A., Ramadhoni, T. S., Prakoso, A. T., Ammarullah, M. I., and Vincent, .., 2019, "The Analysis of the Dimple Arrangement of the Artificial Hip Joint to the Performance of Lubrication," *IOP Conference Series: Materials Science and Engineering*, Vol. 620, p. 012116.
- [86] Gao, L., Yang, P., Dymond, I., Fisher, J., and Jin, Z., 2010, "Effect of Surface Texturing on the Elastohydrodynamic Lubrication Analysis of Metal-on-Metal Hip Implants," *Tribol. Int.*, **43**(10), pp. 1851–1860.
- [87] Gao, L. M., Meng, Q. E., Liu, F., Fisher, J., and Jin, Z. M., 2010, "The Effect of Aspherical Geometry and Surface Texturing on the Elastohydrodynamic Lubrication of Metal-on-Metal Hip Prostheses Under Physiological Loading and Motions," *Proc. Inst. Mech. Eng. Part C J. Mech. Eng. Sci.*, **224**(12), pp. 2627–2636.
- [88] Gao, L., Hua, Z., Hewson, R., Andersen, M. S., and Jin, Z., 2018, "Elastohydrodynamic Lubrication and Wear Modelling of the Knee Joint Replacements With Surface Topography," *Biosurf. Biotribol.*, **4**(1), pp. 18–23.
- [89] Cuervo, P., López, D. A., Cano, J. P., Sánchez, J. C., Rudas, S., Estupiñán, H., Toro, A., and Abdel-Aal, H. A., 2016, "Development of Low Friction Snake-Inspired Deterministic Textured Surfaces," *Surf. Topogr. Metrol. Prop.*, **4**(2), p. 024013.
- [90] Wei, X., Li, W., Liang, B., Li, B., Zhang, J., Zhang, L., and Wang, Z., 2016, "Surface Modification of Co-Cr-Mo Implant Alloy by Laser Interference Lithography," *Tribol. Int.*, **97**, pp. 212–217.
- [91] Kustandi, T. S., Choo, J. H., Low, H. Y., and Sinha, S. K., 2010, "Texturing of UHMWPE Surface via NIL for Low Friction and Wear Properties," *J. Phys. D. Appl. Phys.*, **43**(1), p. 015301.
- [92] Choudhury, D., Roy, T., Krupka, I., Hartl, M., and Mootanah, R., 2015, "Tribological Investigation of Ultra-High Molecular Weight Polyethylene Against Advanced Ceramic Surfaces in Total Hip Joint Replacement," *Proc. Inst. Mech. Eng. Part J J. Eng. Tribol.*, **229**(4), pp. 410–419.
- [93] Pakhaliuk, V., Polyakov, A., Kalinin, M., and Bratan, S., 2016, "Evaluating the Impact and Norming the Parameters of Partially Regular Texture on the Surface of the Articulating Ball Head in a Total Hip Joint Prosthesis," *Tribol. Online*, **11**(4), pp. 527–539.
- [94] Wang, X., Wang, J., Zhang, B., and Huang, W., 2015, "Design Principles for the Area Density of Dimple Patterns," *Proc. Inst. Mech. Eng. Part J J. Eng. Tribol.*, **229**(4), pp. 538–546.
- [95] Dong, G.-N., Hua, M., Li, J., and Chuah, K. B., 2007, "Temperature Field and Wear Prediction for UHMWPE Acetabular Cup With Assumed Rectangular Surface Texture," *Mater. Des.*, **28**(9), pp. 2402–2416.
- [96] Lilley, E., 1999, "Artificial Joint Bioprosthesis for Mitigation of Wear," p. 13.
- [97] Frey, O., 1977, "Prosthetic Acetabulum," p. 4.
- [98] Legrand, R., 1987, "Prosthesis for Replacement of the Hip's Joint," p. 4.
- [99] Mathys, R., 1989, "Artificial Hip Joint Socket With Hydraulic Head Support," p. 4.
- [100] Yuhta, T., Nishimura, I., Kano, D., Saitou, T., Suzuki, T., and Tanaka, M., 1995, "Wear Resisting Slide Member," p. 11.
- [101] Burkinshaw, B. D., 2000, "Implantable Prosthesis Having Textured Bearing Surfaces," p. 13.
- [102] Grundei, H., and Thomas, W., 2002, "Sliding Partners for Artificial Joint Implants," p. 6.
- [103] Schmid, S. R., 2012, "Textured Surfaces for Orthopedic Implants," p. 18.
- [104] Raeymaekers, B., and Sanders, A., 2018, "Prosthetic Joint," p. 11.
- [105] Serbousek, J., and Bono, F. S., 1999, "Wear Reduced Acetabular Component," p. 11.
- [106] Salehi, A., Harbaugh, M., Sauer, W. L., and Carson, C. P., 2003, "Surfaces and Processes for Wear Reducing in Orthopaedic Implants," p. 18.
- [107] Chan, F. W., and Ochoa, J. A., 2003, "Prosthetic Joints Having Reduced Area Bearing Surfaces and Application Thereof to a Range of Sizes of Prosthetic Joints," p. 23.
- [108] Liao, Y., Hoffman, E., Wimmer, M., Fischer, A., Jacobs, J., and Marks, L., 2013, "CoCrMo Metal-on-Metal Hip Replacements," *Phys. Chem. Chem. Phys.*, **15**(3), pp. 746–756.
- [109] Chou, S. Y., Krauss, P. R., Zhang, W., Guo, L., and Zhuang, L., 1997, "Sub-10 Nm Imprint Lithography and Applications," *J. Vac. Sci. Technol. B Microelectron. Nanom. Struct. Process. Meas. Phenom.*, **15**(6), pp. 2897–2904.
- [110] Ippolito, C., Yu, S., Lai, Y. J., and Bryant, T., 2017, "Process Parameter Optimization for Hot Embossing Uniformly Textured UHMWPE Surfaces for Orthopedic Bearings," *Procedia CIRP*, **65**, pp. 163–167.
- [111] Geiger, M., Roth, S., and Becker, W., 1998, "Influence of Laser-Produced Microstructures on the Tribological Behaviour of Ceramics," *Surf. Coatings Technol.*, **100–101**, pp. 17–22.
- [112] Vilhena, L. M., Sedlaček, M., Podgornik, B., Vižintin, J., Babnik, A., and Možina, J., 2009, "Surface Texturing by Pulsed Nd:YAG Laser," *Tribol. Int.*, **42**(10), pp. 1496–1504.
- [113] Etsion, I., 2005, "State of the Art in Laser Surface Texturing," *ASME J. Tribol.*, **127**(1), pp. 248–253.
- [114] Ezhilmaran, V., Vasa, N. J., and Vijayaraghavan, L., 2018, "Investigation on Generation of Laser Assisted Dimples on Piston Ring Surface and Influence of Dimple Parameters on Friction," *Surf. Coatings Technol.*, **335**, pp. 314–326.
- [115] Ancona, A., Jauregui, C., Döring, S., Röser, F., Limpert, J., Nolte, S., and Tünnermann, A., 2009, "Ultrashort Pulse Laser Drilling of Metals Using a High-Repetition Rate High Average Power Fiber CPA System," *Commercial and Biomedical Applications of Ultrafast Lasers IX*, Vol. 7203, p. 720311.
- [116] Sedlaček, M., Podgornik, B., Ramalho, A., and Cesnik, D., 2017, "Influence of Geometry and the Sequence of Surface Texturing Process on Tribological Properties," *Tribol. Int.*, **115**, pp. 268–273.
- [117] Rajurkar, K. P., Zhu, D., McGeough, J. A., Kozak, J., and De Silva, A., 1999, "New Developments in Electro-Chemical Machining," *Ann. CIRP*, **48**(2), pp. 567–579.
- [118] Kumar, S., Singh, R., Singh, T. P., and Sethi, B. L., 2009, "Surface Modification by Electrical Discharge Machining: A Review," *J. Mater. Process. Technol.*, **209**(8), pp. 3675–3687.
- [119] Melentiev, R., and Fang, F., 2020, "Tailoring of Surface Topography for Tribological Purposes by Controlled Solid Particle Impacts," *Wear*, **444–445**, p. 203164.
- [120] Resendiz, J., Egberts, P., and Park, S. S., 2018, "Tribological Behavior of Multi-Scaled Patterned Surfaces Machined Through Inclined End Milling and Micro Shot Blasting," *Tribol. Lett.*, **66**(4), pp. 1–13.
- [121] Marcon, A. R., Bieber, M., and Caulfield, T., 2018, "Representing a 'Revolution': How the Popular Press Has Portrayed Personalized Medicine," *Genet. Med.*, **20**(9), pp. 950–956.
- [122] Zheng, P., Xu, P., Yao, Q., Tang, K., and Lou, Y., 2017, "3D-Printed Navigation Template in Proximal Femoral Osteotomy for Older Children With Developmental Dysplasia of the Hip," *Sci. Rep.*, **7**(1), p. 44993.
- [123] Haynes, J. A., Stambough, J. B., Sassoon, A. A., Johnson, S. R., Clohisy, J. C., and Nunley, R. M., 2016, "Contemporary Surgical Indications and Referral Trends in Revision Total Hip Arthroplasty: A 10-Year Review," *J. Arthroplasty*, **31**(3), pp. 622–625.
- [124] 2020, "Pre-market Notification 510(K)" [Online], <https://www.fda.gov/medical-devices/premarket-submissions/premarket-notification-510k>, Accessed 22 June 2020.
- [125] Gao, L., Dowson, D., and Hewson, R. W., 2016, "A Numerical Study of Non-Newtonian Transient Elastohydrodynamic Lubrication of Metal-on-Metal Hip Prostheses," *Tribol. Int.*, **93**(Part B), pp. 486–494.
- [126] Paul, J. P., 1966, "Paper 8: Forces Transmitted by the Joints in the Human Body," *Proceedings of the Institution of Mechanical Engineers*, pp. 8–15.